Computers and Electronics in Agriculture 253 (2026) 112179

Contents lists available at ScienceDirect

Computers and Electronics in Agriculture

journal homepage: www.elsevier.com/locate/compag

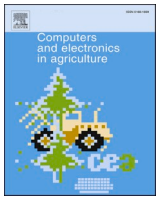

Leaf- and canopy-level hyperspectral sensing of wheat-Fusarium head blight-*Trichoderma gamsii* interactions

Lorenzo Pippi [a,b], Samuele Risoli [a,c,*], Sergio Cogliati [d,e], Matteo Sali [d,e], Roberto Garzonio [d,e], Elisa Pellegrini [a,c], Cristina Nali [a,c], Lorenzo Cotrozzi [a,c]

[a] *Department of Agriculture, Food and Environment, University of Pisa, Pisa, Italy*
[b] *University School for Advanced Studies IUSS, Pavia, Italy*
[c] *Centre for Agri-Environmental Research "Enrico Avanzi" (CiRAA), University of Pisa, Pisa, Italy*
[d] *Remote Sensing of Environmental Dynamics Lab, University of Milano-Bicocca, Milano, Italy*
[e] *Department of Earth and Environmental Sciences, University of Milano-Bicocca, Milano, Italy*

A R T I C L E I N F O

Keywords:
Biocontrol
Early detection
FHB
Multivariate statistics
Reflectance spectroscopy

A B S T R A C T

Fusarium head blight (FHB) is a major mycotoxigenic disease of wheat, causing yield and quality losses and deoxynivalenol contamination. Rapid, non-destructive tools are needed to detect FHB, monitor wheat physiological responses, and evaluate sustainable management strategies, including biological control agents. Although vegetation spectroscopy is widely used for high-throughput phenotyping, most spectral studies focus on binary disease detection, while the capacity of hyperspectral data to capture concurrent host–pathogen–biocontrol responses across leaf and canopy scales remains underexplored. Here, we tested a full-range (400–2400 nm) hyperspectral phenotyping framework to track early interactions among winter wheat, FHB, and *Trichoderma gamsii* T6085. Two cultivars, Bingo and Rebelde, with higher and lower FHB susceptibility, respectively, were treated with a chemical fungicide (Chem) or *T. gamsii* T6085 (Bioc) under FHB pressure. Leaf- and canopy-level spectra were acquired at 2, 5, and 14 days post-inoculation, alongside gas exchange, water status, and chlorophyll measurements. Permutational multivariate analysis of variance (PERMANOVA) tested whole-spectrum effects, partial least squares discriminant analysis (PLS-DA) explored class separability, and partial least squares regression (PLSR) estimated physiological traits. PERMANOVA detected genotype × inoculation × treatment interactions from 5 days post-inoculation at leaf and canopy levels. PLS-DA revealed treatment- and cultivar-dependent spectral fingerprints, but overall low-to-fair validation performance indicates that these class-specific patterns should be interpreted as exploratory and not as evidence of operational treatment discrimination. PLSR provided high accuracy for chlorophyll content and osmotic potential, moderate accuracy for CO_2-assimilation traits, and poor accuracy for transpiration and leaf water potential. While the workflow is scalable as an experimental and analytical framework, its operational deployment will require broader validation across sites, seasons, cultivars, disease-pressure conditions, and sensing platforms.

1. Introduction

Winter wheat (*Triticum aestivum* L.) is one of the most important staple crops globally, providing approximately 20 % of the total dietary calories consumed worldwide and playing a central role in food security and economic stability (Erenstein et al., 2022). Despite its importance, wheat production is increasingly threatened by fungal diseases that severely compromise yield and grain quality. Among these, Fusarium head blight (FHB) represents one of the most destructive diseases affecting wheat worldwide, causing substantial economic losses through yield reduction and quality deterioration (Dean et al., 2012; Alisaac and Mahlein, 2023). Although *Fusarium graminearum* is the primary causal agent, several other species belonging to *F. graminearum* species complex can also induce the disease, either individually or in combination (Khan et al., 2020; Risoli et al., 2024). The destructive impact of FHB is largely attributable to the production of mycotoxins (i.e., secondary toxic metabolites synthesized by mycotoxigenic *Fusarium* species). Among these, deoxynivalenol (DON) is one of the most prevalent and harmful

* Corresponding author.
E-mail address: samuele.risoli@unipi.it (S. Risoli).

https://doi.org/10.1016/j.compag.2026.112179
Received 24 March 2026; Received in revised form 25 June 2026; Accepted 8 July 2026
Available online 15 July 2026

contaminants of wheat grain (EFSA, 2017; Dweba et al., 2017; Rypar et al., 2025) posing serious acute and chronic health risks to both humans and livestock (Krska et al., 2001). The incidence and severity of FHB have increased in recent decades, driven by climate change and the expansion of wheat cultivation into new agroecological zones. These trends further emphasize the urgency of developing effective and sustainable strategies to protect global wheat production (McMullen et al., 2012; Dweba et al., 2017; Kos et al., 2023).

Managing FHB and mitigating DON contamination remain particularly challenging due to the pathogen's broad environmental adaptability and its capacity to infect multiple cereal hosts (McMullen et al., 2012; Steiner et al., 2017). Conventional management strategies rely on integrated approaches that include crop rotation, the use of resistant wheat varieties, and fungicide applications (McMullen et al., 2012). However, these measures often provide only partial control and raise concerns regarding long-term sustainability, particularly due to the emergence of fungicide resistance and the environmental impact associated with repeated chemical inputs (McMullen et al., 2012; Alisaac and Mahlein, 2023). Recently, biological control agents (BCAs) have gained primary importance as key components of integrated disease management strategies (Risoli et al., 2024). Biocontrol agents – including species of bacteria, yeasts and filamentous fungi – can suppress FHB by competing with the pathogen for nutrients and space, producing antifungal metabolites, or inducing plant defence mechanisms (Legein et al., 2020; Risoli et al., 2022, 2024). The appeal of BCAs lies in their environmentally friendly nature and their capacity to target pathogens through multiple, complementary mechanisms (Bonaterra et al., 2022; Risoli et al., 2023). Unlike conventional fungicides, which typically rely on a single mode of action, BCAs can simultaneously inhibit pathogen growth, reduce the accumulation of harmful mycotoxins, and enhance host plant immunity (Risoli et al., 2023, 2024, 2025). Despite their promise, BCA efficacy is often variable and strongly influenced by environmental conditions – such as temperature, humidity, and soil composition – which affect both the pathogen and the BCA (Butt and Copping, 2000). Crucially, BCA performance is also tightly linked to the timing of application, underscoring the need for precise intervention windows to maximize FHB suppression (Ons et al., 2020; Risoli et al., 2024). However, achieving such precision remains challenging, as conventional disease monitoring approaches become impractical when applied to large plant populations spanning diverse phenological stages and broad geographic scales (Alisaac and Mahlein, 2023). This logistical bottleneck has catalyzed interest in the development of rapid, high-throughput, and sustainable sensing strategies capable of accurately monitoring FHB while simultaneously capturing wheat physiological responses to the pathogen.

Recent advancements in the sensitivity and portability of spectroradiometers, together with substantial improvements in computational capacity and chemometric modelling, have unlocked the potential of hyperspectral reflectance data through several complementary analytical approaches. First, vegetation indices (VIs) derived from the ratios or combinations of reflectance at specific wavelengths have been widely used to predict vegetation traits (e.g., normalized difference vegetation index, NDVI; Gamon et al., 1995). Second, multivariate statistical methods (e.g., partial least squares regression, PLSR; Wold et al., 2001) enable the direct estimation of key foliar morphological, physiological, and biochemical traits from spectral signatures (e.g., Serbin et al., 2015; Couture et al., 2018; Cotrozzi et al., 2017, 2020a, 2020b). Third, reflectance spectra can be interpreted holistically as phenotypic expression integrating chemical, morphological, and physiological leaf properties under specific environmental conditions (i.e., analyses of spectral signatures; Cotrozzi and Couture, 2020).

Within this framework, hyperspectral sensing has emerged as a powerful, high-dimensional tool for the early detection and monitoring of both biotic (Gongora-Canul et al., 2020; Cotrozzi, 2022) and abiotic (Briglia et al., 2020; Cotrozzi et al., 2017, 2018, 2020; Cotrozzi and Couture, 2020) stress factors. This non-invasive technique exploits the optical properties of vegetation – at both leaf and canopy scale – to generate information-rich datasets capable of detecting subtle physiological, biochemical, and morphological changes, often before visible symptoms appear (Carli et al., 2025; Cotrozzi, 2022). Recent advancements in computational capacity and chemometric modeling have unlocked the ability to exploit these high-dimensional reflectance spectra through a range of analytical frameworks.

While hyperspectral sensing offers transformative potential for precision agriculture and sustainable wheat production (Mahlein et al., 2024), its application to complex disease-management systems remains less developed than conventional binary disease detection. Current research has demonstrated that these technologies can enhance FHB management by identifying infection-related physiological shifts before visible symptoms appear, thereby enabling timely interventions (Alisaac and Mahlein, 2023; Mahlein et al., 2024). However, in FHB management, the key challenge is not only to distinguish infected from healthy plants, but also to monitor plant functional status and treatment-dependent responses within the narrow intervention window in which control strategies are most effective (Alisaac and Mahlein, 2023; Mahlein et al., 2024). This capability is particularly critical for the success of BCAs, which must be applied early in the infection cycle to achieve optimal efficacy (Risoli et al., 2024). Moreover, BCA efficacy is strongly influenced by application timing and environmental conditions, making dynamic monitoring of plant health and treatment response especially relevant (Risoli et al., 2024). However, a significant knowledge gap persists regarding the use of spectral data to monitor and interpret the complex tri-trophic interactions among the host plant, the pathogen, and the biocontrol agent, which are known to have important ecological and agricultural implications (Agrawal, 2000). In this context, "tri-trophic interactions" are operationally defined as the integrated spectral and physiological response of the host plant to the factorial combination of genotype, FHB inoculation, and management treatment. Hyperspectral reflectance is therefore not expected to directly isolate separate optical signals from the plant, pathogen, and biocontrol agent, but to capture the resulting plant phenotypic fingerprint generated by their combined effects. Characterizing the concurrent spectral signatures associated with disease progression and BCA-induced responses, often occurring at different spatial scales, represents a major technical challenge that has yet to be fully addressed. In this context, hyperspectral sensing is particularly suitable because full-range reflectance integrates information on pigments, water status, leaf structure, and biochemical composition, thus providing a rapid and non-destructive readout of plant health across both leaf and canopy scales (Alisaac and Mahlein, 2023; Cotrozzi, 2022). Integrating hyperspectral information across leaf and canopy levels provides a promising avenue to bridge individual physiological responses with field-scale dynamics. Nevertheless, limited field-based evidence is available on whether hyperspectral signatures can capture the combined effects of host genotype, FHB infection, and management treatment, or discriminate the physiological fingerprints associated with chemical and biological control strategies. Such a multi-scale approach is essential to assess whether sustainable disease management strategies, such as BCA applications, can be reliably monitored and optimized under field conditions, ultimately reducing reliance on conventional fungicides and supporting long-term food security (Lahlali et al., 2022; Alisaac and Mahlein, 2023; Mahlein et al., 2024). Addressing this gap is essential to move beyond simple healthy-versus-infected classification and toward spectral monitoring approaches that can support both disease surveillance and the evaluation of phytosanitary treatment performance under realistic field conditions. Accordingly, the analytical workflow was structured to address linked biological questions rather than to apply independent statistical tools. First, whole-spectrum analyses were used to test whether genotype, FHB inoculation, treatment, and their interactions altered the spectral phenotype of wheat plants, following the interpretation of reflectance spectra as integrated phenotypic expressions of plant physiological, biochemical, and structural properties (Cotrozzi and Couture, 2020).

Second, exploratory classification was used to evaluate whether these spectral differences translated into separable treatment- or cultivar-dependent fingerprints, in line with the use of multivariate classification approaches for high-dimensional spectral datasets (Kuhn, 2008; Couture et al., 2018). Third, regression and clustering approaches were used to relate spectral variation to physiological traits and to interpret the underlying plant functional responses, consistent with spectra-trait modeling and multivariate pattern interpretation frameworks previously applied in plant phenotyping studies (Altman and Krzywinski, 2017; Cotrozzi et al., 2020; Cotrozzi and Couture, 2020; Serbin et al., 2015).

Therefore, this study aimed to explore the potential of full-range (400–2400 nm) hyperspectral sensing as a high-throughput phenotyping tool for early monitoring of wheat–FHB–biocontrol interactions under field conditions. Two winter wheat cultivars, Bingo and Rebelde, characterized by higher and lower susceptibility to FHB, respectively, were selected to provide a controlled contrast in host susceptibility within the factorial design, rather than to represent the full genetic diversity of wheat, treated with either conventional systemic agrochemicals (Binal Pro, tetraconazole and prochloraz; Chem) or *Trichoderma gamsii* T6085 (Bioc; a well-established biocontrol agent effective against FHB; Risoli et al., 2023) and either inoculated or not with the pathogen. Specifically, this study aimed to (i) assess whether leaf- and canopy-level spectra can resolve complex Genotype × Inoculation × Treatment dependant spectral responses over time in a wheat-FHB-BCA system, (ii) develop and validate PLSR models for non-destructive prediction of key functional traits related to plant health status (e.g., gas exchange, water status, and chlorophyll content) in winter wheat using leaf spectra, and (iii) identify spectral regions and vegetation indices that most effectively describe treatment-dependent phenotypic fingerprints associated with chemical and biological control under FHB pressure.

2. Materials and methods

2.1. Experimental site and setup

The experimental activities were carried out during the 2021–2022 cropping season at the "Podere Rottaia" field stations of the University of Pisa (San Piero a Grado, Pisa, Italy; 43.674 N, 10.318 E, 0 m a.s.l.). The site is characterized by a typical Mediterranean climate, with average annual maximum and minimum daily temperatures of 19.3 and 11.3 °C, respectively, and a mean rainfall of 971 mm per year [climatic data were obtained from the TOS01005251 automatic meteorological station of Tuscany Region (historical series: 1995–2023; https://www.sir.toscana.it/)]. Daily minimum, medium and maximum air temperatures and rainfall were recorded throughout the entire experimental period corresponding to the winter wheat growing cycle (November 2021 – June 2022). During this period, total precipitation amounted to 565 mm, distributed over 49 rainy days and mainly concentrated between November and December. The average daily maximum and minimum temperatures were 20.6 and 12.3 °C, respectively.

Winter wheat (*T. aestivum* cvs. Bingo and Rebelde) was sown at the end of November 2021 at a density of 250 seeds m^{-2} in 48 plots (6 × 1.5 m). Each plot was subdivided into four subplots (3 × 0.75 m) and separated by 2-m wide buffer zones to minimize interplot interference. The experiment was arranged in a random complete block design (4 replications, Fig. S1). For each cultivar, six experimental conditions were randomly assigned within each block (see below for further details): (i) untreated (i.e., sprayed with a mock solution) and not-inoculated (Mock/FHB-, i.e., control), (ii) untreated and inoculated with FHB agents (Mock/FHB+), (iii and iv) treated with Chem or Bioc and not-inoculated (Chem/FHB- or Bioc/FHB-, respectively), and (v and vi), treated with Chem or Bioc and inoculated with FHB agents (Chem/FHB+ or Bioc/FHB+, respectively). All preliminary field operations (i.e., fertilization management, fungal material preparation, spike treatments, pathogen (i.e., *Fusarium graminearum* ITEM124 and *F. langsethiae* ITEM 11031) inoculation procedures, and disease assessment), including the previously reported FHB data, were performed as described in Risoli et al. (2025).

2.2. Collection of leaf and canopy spectra

Hyperspectral measurements were acquired at both leaf and ground-canopy scales using an ASD FieldSpec 4 HR spectroradiometer (350–2,500 nm; Analytical Spectral Devices, Boulder, CO, USA). For leaf measurements, the fiber optic was mounted on a plant probe equipped with a leaf-clip incorporating an internal halogen source (Cotrozzi et al., 2020). On each plant, two 1-cm-diameter spots were randomly selected on the adaxial surface of the youngest fully expanded leaf (one spectrum per spot) at full flowering stage (BBCH 65; 50 % of anthers mature). One spectrum was collected per spot, and the two spectra were averaged to obtain a single representative spectrum per leaf/plant. Canopy spectra were collected under clear-sky conditions between 11:00 and 13:00 am using the fiber optic attached to a pistol grip held approximately 1 m above the canopy, with the foreoptic oriented near nadir. To minimize illumination-related variability during field canopy acquisitions, white-reference calibration was performed before measuring each plot. This configuration yielding a footprint of approximately 10 cm^2 per measurement. For canopy measurements, a 99 % Spectralon® diffuse reflectance panel (Labsphere, Inc., North Sutton, NH, USA) was used as the white reference, whereas for leaf measurements, the internal white reference of the leaf-clip was used. White and dark reference measurements were repeated every ten spectra. Both leaf and canopy spectra were collected at 2-, 5-, and 14-days post inoculation (dpi), intervals chosen in accordance with preliminary observations of the disease progression. Relative reflectance was computed as the dark-corrected sample/white ratio assuming a unit reflectance of the white reference (Eq. (1) and expressed as a percentage. All analyses used untransformed reflectance data, applying only detector-join ("spectral jump") correction and interpolation to a common wavelength grid. Overall, four spectra per plant were acquired across leaf and canopy measurements, resulting in a total of 1,068 leaf spectra and 604 canopy spectra.

$$R(\lambda) = \frac{L_{target}(\lambda) - L_{dark}(\lambda)}{L_{white}(\lambda) - L_{dark}(\lambda)};\ R_{\%}(\lambda) = R(\lambda) \times 100 \quad (1)$$

- $L_{target}(\lambda) = target(leaf/canopy)spectralradiance/instrumentsignal$,
- $L_{white}(\lambda) = white - referencespectralradiance/instrumentsignal$,
- $L_{dark}(\lambda) = darksignal$.

2.3. Standard measurements

2.3.1. Analysis of gas exchange and chlorophyll content

Net photosynthesis (A), transpiration (E), stomatal conductance (g_s), and intercellular CO_2 concentration (C_i) were measured using a portable LI-6400 gas exchange system (Li-Cor, Inc., Lincoln, NE, USA) equipped with a 2 × 3 cm chamber and a 6400-02B LED light source. Measurements were conducted at an ambient CO_2 concentration of 400 ppm, at room temperature (25 ± 3 °C), and saturating light (1,500 µmol m^{-2} s^{-1} PAR; Quaratiello et al., 2024). Instantaneous water use efficiency (WUE_i) was calculated as A/E. Intrinsic water use efficiency (WUE_{in}) was calculated as A/g_s. Each leaf used for gas exchange measurements was also analyzed using SPAD 502 chlorophyll meter (Minolta, Osaka, Japan), which provides a rapid and non-invasive estimate of chlorophyll content (Chl_{SPAD}) based on leaf greenness. For each sample, three measurements were taken, and the average value was recorded. Measurements were taken under stable environmental conditions, avoiding hours of excessive heat or irradiance (e.g., the hottest midday hours) that could induce transient stress responses in the leaves.

Table 1
Vegetation indices calculated from leaf and canopy hyperspectral reflectance spectra. For each index, the table reports the name, formula, and reference.

Index	Formula	Reference
NDVI	$(R_{780}\text{-}R_{570})/(R_{780} + R_{570})$	Gamon et al., 1995
NDLI	$\log(1/R_{1754}) - \log(1/R_{1680})]/[\log(1/R_{1754}) + \log(1/R_{1680})$	Serrano et al. 2002
NDWI	$(R_{860}\text{-}R_{1240})/(R_{860} + R_{1240})$	Gao, 1996
ARI	$(R_{550})^{-1}\text{-}(R_{700})^{-1}$	Gitelson et al., 2001

2.3.2. Water status analysis

Leaf water potential (Ψ_W) was measured using a Scholander PMS 600 pressure chamber (PMS Instrument Company, Albany, OR, USA), following the standard protocol described by Tiekstra et al. (2000). To determine leaf osmotic potential (Ψ_π), a leaf portion (about 2 × 2 cm) was placed into a microtube, immersed in liquid nitrogen, and then stored at −80 °C until analysis. The solute concentration was then determined with a Wescor 5500 vapor pressure osmometer (Wescor, Logan, UT, USA; Pisuttu et al., 2023).

2.4. Analyses of spectral signatures

The statistical workflow followed a sequential rationale: PERMANOVA and PCoA were first used to test and visualize whole-spectrum responses to the experimental factors; PLS-DA was then used to explore the separability of significant spectral effects; PLSR was applied to estimate physiological traits from spectra; and vegetation indices and clustering were finally used to support the biological interpretation of treatment- and genotype-dependent responses. The effects of genotype (G), inoculation (I), treatment (T), and their interactions (i.e., 'G' × 'I', 'G' × 'T', 'I' × 'T', 'G' × 'I' × 'T') on leaf- and canopy-level reflectance profiles of wheat plants were assessed by permutational analysis of variance (PERMANOVA, a non-parametric method base on permutation tests; Anderson, 2001). Analyses were performed using Euclidian measurements of dissimilarity and 10,000 permutations. Euclidean distance was selected because spectra consisted of continuous reflectance variables acquired on a common wavelength grid; PERMANOVA outputs were therefore interpreted as whole-spectrum dissimilarities, considering the sensitivity of distance-based methods to multivariate dispersion. Spectral responses were visualized by principal coordinates analysis (PCoA) applied to the same spectral datasets utilized for PERMANOVA, using the'vegan' package in R (https://www.r-project.org), accessed on 26 September 2024; (Dixon, 2003). Principal coordinates analysis reduces data dimensionality by projecting the original variables into a set of uncorrelated variables. Using Euclidean distance matrices, PCoA was run only for the effects found to be significant by PERMANOVA. Partial least squares discriminant analysis (PLS-DA; Chevallier et al., 2006) was additionally used to determine the ability of hyperspectral data to sort experimental groups that showed statistical significance by PERMANOVA. PLS-DA is a statistical approach used with high dimensional data to discriminate groups by projecting latent variables through the response and predictor variables to both reduce data dimensionality and maximize prediction accuracy. In addition, this method is largely exploited when predictor variables have a high degree of collinearity. The PLS model fits response variables that are indicators of groups of interest to the spectrum (Cotrozzi and Couture, 2020). No algorithmic modification of PLS-DA was performed; instead, model optimization was based on calibration:validation partitioning and latent-variable selection. Specifically, the analyses were run 500 times by iteratively splitting observations into different groups of calibration (training) and validation (testing) subsets. Classification accuracy was assessed based on the number of correct classifications in both calibration and the validation sets. The calibration:validation data ratio and the number of components (i.e., latent variables) used to obtain the models that would give the highest exploratory PLS-DA classification performance were determined by iteratively running the PLS-DA models with different calibration:validation data ratios (i.e., 50:50, 70:30, and 80:20), and numbers of components and was based on the highest *Kappa* values returned for the validation models. Because some optimized models required a relatively high number of latent variables, PLS-DA outputs were interpreted only as exploratory indicators of spectral class separability rather than as parsimonious operational classifiers. PLS-DA was performed in R using the'caret' and'vegan' packages (https://www.r-project.org, accessed on 26 September 2024; Dixon, 2003; Kuhn, 2008).

2.5. Plsr-model calibration and validation

PLSR (Wold et al., 2001) models were developed from the reflectance profiles to predict A, E, g_s, C_i, WUE_i, WUE_{in}, Chl_{SPAD}, Ψ_W and Ψ_π. When predictor variables are highly correlated (as in the case of hyperspectral data) conventional regression techniques can produce unreliable coefficients and error estimates. Conversely, PLSR reduces many collinear predictor variables into relatively few, uncorrelated latent variables and has become the preferred method for chemometric approaches (Cotrozzi and Couture, 2020). To avoid potential overfitting, the numbers of components (i.e., latent variables) in the PLSR models were selected based on the reduction of the predicted residual sum of squares (PRESS) statistics (Chen et al., 2004), using leave-one-out-cross-validation. The selected sets of extracted components were then combined into linear models predicting leaf traits based on leaf spectral profiles. Similarly to PLS-DA, the model performance was evaluated by conducting 500 randomized permutations of the datasets iteratively using 80 % of the data for calibration and the remaining 20 % for validation. For each permutation, model performance was assessed for both calibration and validation datasets using the goodness-of-fit model (R^2), the overall error rate (i.e., root mean square error, RMSE), the percentage of RMSE over the data range (%RMSE), and the bias. The strength contribution of PLSR loadings by individual wavelengths was also determined using the variable importance in projection (VIP) statistics (Wold et al., 2001; Chong and Jun 2005). The VIP scores evaluate the importance of individual wavelengths in explaining the variation in both the predictor and response variables, with larger weightings conferring greater value to the contribution of individual wavelengths to the predictive model (Cotrozzi and Couture, 2020). Before developing the final modeling, preliminary PLSR analyses were conducted to identify poorly predicted predicted observations as a quality-control step, following established spectra-trait modeling workflows (i.e., outliers; Cotrozzi et al., 2018, 2020; Cotrozzi and Couture, 2020; Couture et al., 2018; Serbin et al., 2015). Prediction residuals were examined, and potential outliers were further checked for spectral artefacts and extreme reference values. Removed outliers accounted for approximately 11 % of the initial dataset. All modeling and statistical analyses were performed in R using the'pls' package (https://www.r-project.org, accessed on 26 September 2024). In accordance with best practices, the final PLSR models were further evaluated through external validation (i.e., test their accuracy in prediction on other independent samples not used in model development). Model coefficients were applied to an independent dataset not used for model calibration and internal validation (ca. 20 % of the whole dataset). Relations between predicted and observed values were tested by regression analysis, and fit statistics (i.e. R^2, RMSE, bias) were again used to assess model estimation accuracy. No methodological modification of the PLSR algorithm was introduced; model development relied on optimization of the spectral region and number of latent variables for each target trait.

2.6. Estimation of leaf traits by vegetation indices and PLSR-models

Four common vegetation indices were calculated from spectra (Table 1): the normalized difference vegetation index (NDVI) was determined to estimate the potential occurrence of (sub)visible symptoms; the normalized difference lignin index (NDLI) was determined to estimate the relative amount of lignin in leaves and canopy; the normalized difference water index (NDWI) was determined to estimate changes in leaf water content and the anthocyanin reflectance index (ARI) was calculated for the accumulation of anthocyanin as defense response. R_x indicates reflectance at x nm wavelength. Other leaf traits were estimated from spectra by using the best performing PLSR-models. As already stated above, vegetation indices and spectra-derived leaf traits were calculated from spectra averaged per plant.

2.7. Statistical analysis of leaf traits derived from spectra

All collected samples were analyzed together, using the plant as experimental unit. The Shapiro-Wilk test was first used to assess the normal distribution of spectral indices and leaf traits derived from spectra by PLSR-models. The effects of 'G', 'I', 'T', and their interactions (i.e., 'G' × 'I', 'G' × 'T', 'I' × 'T', 'G' × 'I' × 'T') on these leaf and ground-canopy traits were then investigated by a three-way repeated measures analysis of variance (ANOVA). Tukey's test was used as post-hoc test. Statistically significant effects were considered for $P \leq 0.05$. Univariate statistical analyses were run in JMP Pro 14.0.0 (SAS Institute Inc., Cary, NC, USA). To visualize overall physiological response patterns and to group experimental conditions based on trait similarity, Hierarchical Cluster Analysis was performed. Prior to clustering, data were standardized as Z-scores (mean centering and scaling to unit variance) to ensure comparability across the different measurement units of the spectral indices and traits. The analysis was conducted considering Euclidean distances and applying Ward's linkage rule to both rows (experimental treatments) and columns (measured traits; Altman and Krzywinski, 2017).

3. Results

3.1. Characterization of leaf and canopy spectral signatures

Average spectral profiles of wheat leaves and ground-canopy measurements (regardless of the experimental condition) are shown in Fig. 1. For both leaf and ground-canopy-level spectra, the largest variability in reflectance profiles generally coincided with typical features of vegetation reflectance, including the reflectance peak around 550 nm in the VIS, throughout the NIR (800 − 1300 nm) characterized by high reflectance values, and peaks in the SWIR region centered at 1700, 1800 and 2200 nm.

3.2. Analyses of spectral signatures collected at leaf level

First, multiple spectral ranges were investigated to optimize the statistical outputs of the PERMANOVA for the effects of 'G', 'I', and 'T', and their interactions at 2-, 5- and 14-days dpi. The best output was recorded using the full range profile (i.e., 400–2400 nm).

At the leaf-level, three-way PERMANOVA showed a significant effect of 'G' (*df*: 1) and'I' (*df*: 1) on hyperspectral profiles collected at 2 dpi, a significant effect of 'G' and of the three-way interaction among all factors (i.e, 'G' × 'I' × 'T'; *df*: 2) at 5 dpi. Finally, significant effect of 'G', its interaction with 'T' (i.e., 'G' × 'T'; *df*: 2) and the full three-way

Table 2
F and P *values of three-way permutational multivariate analysis of variance for the effects of genotype (G), inoculation (I), treatment (T), and their interaction* (i.e., *G × I, G × T, I × T, G × I × T) on the full-range (400–2,400 nm) reflectance profiles of wheat plants collected at leaf-level at 2, 5 and 14 days post inoculation (dpi).* df *represents degrees of freedom.* *** $P \leq 0.001$, ** $P \leq 0.01$, * $P \leq 0.05$; ns: $P > 0.05$.

TIME	EFFECT	*df*	F	*P*
2 dpi	**G**	**1**	**23.32**	***
	I	**1**	**3.59**	*
	T	2	0.35	ns
	G × I	1	0.16	ns
	G × T	2	0.95	ns
	I × T	2	1.89	ns
	G × I × T	2	1.13	ns
5 dpi	**G**	**1**	**89.29**	***
	I	1	2.21	ns
	T	2	1.45	ns
	G × I	1	1.57	ns
	G × T	2	0.12	ns
	I × T	2	2.12	ns
	G × I × T	**2**	**2.68**	*
14 dpi	**G**	**1**	**53.11**	***
	I	1	1.22	ns
	T	2	1.40	ns
	G × I	1	1.38	ns
	G × T	**2**	5.14	**
	I × T	2	1.41	ns
	G × I × T	**2**	**21.96**	***

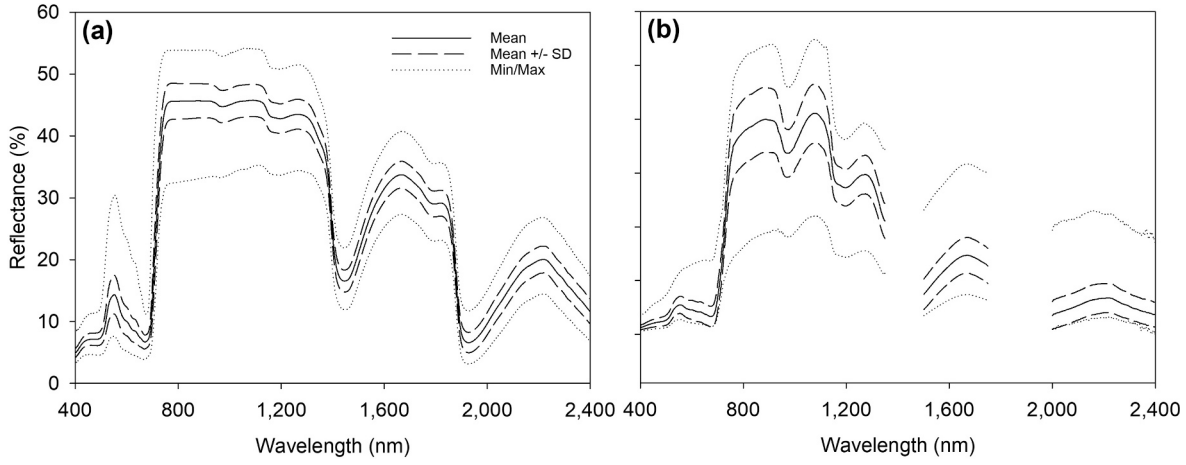

Fig. 1. *Summary of leaf (a) and ground-canopy (b) spectral measurements repeatedly collected from winter wheat cultivars Rebelde and Bingo. Plants were treated with water, conventional agrochemical and* Trichoderma gamsii *T6085 and inoculated or not with* Fusarium graminearum *ITEM124 and* F. langsethiae *ITEM 11031. Measurements were performed at 2-, 5- and 14-days post-inoculation, and devoted to the analyses of spectral signatures. The mean, mean ± standard deviation (SD), minimum and maximum leaf and canopy reflectance profiles are shown for all samples (n = 840 and 470 at leaf and ground-canopy level, respectively).*

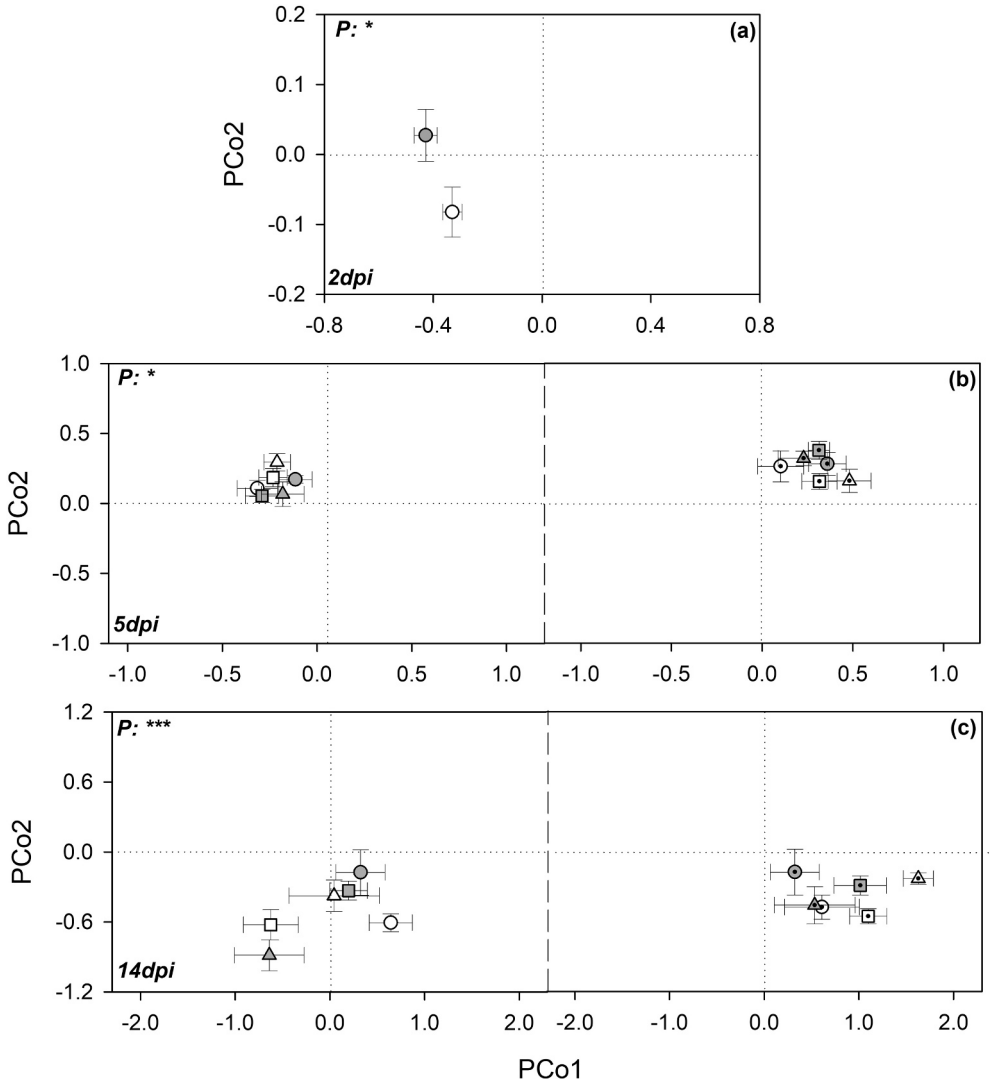

Fig. 2. *Scores (mean ± standard error) for the first and second principal components from principal coordinates analysis (PCoA) of reflectance data (400–2,400 nm) collected from wheat plants at leaf-level on Rebelde and Bingo winter wheat cultivars treated with water (Mock), systemic agrochemical (Chem) and* Trichoderma gamsii *T6085 (Bioc) and inoculated (FHB-) or not (FHB+) with* Fusarium graminearum *ITEM124 and* F. langsethiae *ITEM 11031 at 2 (**a**), 5 (**b**) and 14 (**c**) days post inoculation (dpi). (**a**) White and grey circles represent scores for FHB- and FHB+ plants (regardless of the cultivar), respectively. (**b** and **c**) White and grey shapes represent scores for FHB- and FHB+ plants, respectively, treated with Mock (circles), Chem (square) and Bioc (triangles). Empty and dotted symbols represent the Rebelde and Bingo cultivars (left and right sub-panel, separated by the dashed vertical line, respectively).* P *value from permutational analysis of variance on full range (400–2,400 nm) reflectance profiles of wheat leaves are shown on the top right corner of panels (***:* $P \leq 0.001$*; *:* $P \leq 0.05$*).*

interaction of 'G' × 'I' × 'T' (*df*: 2) at 14 dpi (Table 2).

At 2 dpi, the highest exploratory PLS-DA classification performance for 'I' from the spectra (i.e., higher mean *Kappa*) using PLS-DA was detected with an 80:20 calibration:validation ratio and 10 latent components. Accuracy and *Kappa* for the validation were 0.55 and 0.10, respectively (Fig. 2a; Table S1). Finally, the confusion matrix obtained by PLS-DA shows the accuracy of discrimination for single category of leaf spectra at 2 dpi (Table S2).

At 5 dpi, average spectral profiles of Rebelde and Bingo plants subjected to Chem/Bioc treatments and either inoculated or not with FHB are visualized in Fig. 2b. The highest average *Kappa* of three-way interaction (i.e., 'G' × 'I' × 'T') using PLS-DA was detected with an 80:20 calibration:validation ratio, using 40 components. Accuracy and *Kappa* for the validation were 0.30 and 0.27, respectively (Table S3) and the highest accuracies (> 40 %) were achieved for the discrimination of Rebelde spectral responses in Chem/FHB-, Mock/FHB+, and Chem/FHB+ plants, as shown in the confusion matrix obtained by PLS-DA at 5 dpi (Table S4).

Finally, at 14 dpi, average spectral profiles of Mock/FHB-, Mock/FHB+, Chem/FHB-, Chem/FHB+, Bioc/FHB-, and Bioc/FHB+ plants of Rebelde and Bingo were visualized in Fig. 2c. The higher mean *Kappa* classification of the three-way interaction (i.e., 'G' × 'I' × 'T') from the spectra by PLS-DA was detected with an 80:20 calibration:validation ratio and 30 components. Accuracy and *Kappa* for the validation were 0.36 and 0.30, respectively (Table S5). The highest class-specific accuracies (> 40 %) was observed for the discrimination of Rebelde Chem/FHB-, and Bingo Mock/FHB+, with values exceeding 65 % for Chem/FHB- and Bioc/FHB-. However, overall validation performance remained low to fair, with *Kappa* values below 0.40. The confusion matrix obtained by PLS-DA, for leaf hyperspectral profiles, shows the accuracy of discrimination for single category at 14 dpi (Table S6).

3.3. Analyses of spectral signatures collected at ground-canopy level

Multiple spectral ranges were initially investigated to optimize the statistical outputs of PERMANOVA at 2, 5, and 14 dpi. The best outputs were obtained using the full range (i.e., 400–2,400 nm; Table 3). Spectral ranges 1,300–1,500 nm and 1,800–2,000 nm were excluded to

minimize signal noise associated with atmospheric water vapor (Fig. 1b).

At ground-canopy level, three-way PERMANOVA showed a significant effect of 'I' × 'T' (*df*: 1) on hyperspectral profiles collected at 2 dpi, a significant effect of 'G' (*df*: 1), 'T' (*df*: 2) and of the three-way interaction of all factors (i.e, 'G' × 'I' × 'T'; *df*: 2) at 5 dpi and, finally, significant effect of 'G' (*df*: 1) 'T' (*df*: 2) and their double interaction (i.e., 'G' × 'T'; *df*: 2) at 14 dpi (Table 3).

At 2 dpi, average spectral profiles of wheat plants (regardless of the cultivar) subjected to Chem/Bioc treatments and either inoculated or not with FHB were visualized in Fig. 3a. The best classification of the double interaction (i.e., 'I' × 'T'; *df*: 1) from the spectra (i.e., higher mean *Kappa*) using PLS-DA was detected with an 80:20 ratio for calibration:validation data, using 20 components. Accuracy and *Kappa* for the validation were 0.30 and 0.16 (Table S7). As shown in Table S8, the highest accuracy (40 %) was achieved for the discrimination of Chem/FHB+ wheat plants.

At 5 dpi, average spectral profiles of wheat plants subjected to Chem/Bioc treatments and either inoculated or not with FHB were visualized in Fig. 3b. The best classification of the three-way interaction (i.e., 'G' × 'I' × 'T') from the spectra (i.e., higher mean *Kappa*) using PLS-DA was detected with an 80:20 ratio for calibration:validation data, using 50 components. Accuracy and *Kappa* for the validation were 0.32 and 0.24 (Table S9). The highest accuracies (> 50 %) were achieved for the discrimination of Rebelde Mock/FHB+ and Chem/FHB+ plants (Table S10).

Finally, at 14 dpi, average spectral profiles of Rebelde and Bingo plants (regardless of the infection) subjected to Chem/Bioc treatments were visualized in Fig. 3c. The higher average *Kappa* of the double interaction (i.e., 'G' × 'T', *df*: 1) from the spectra by PLS-DA was detected with an 80:20 ratio for calibration:validation data. Accuracy and *Kappa* for the validation were 0.45 and 0.29, respectively, using 18 components (Table S11). Some class-specific accuracies exceeded 60 %, particularly for Rebelde Mock and Chem plants, although overall validation performance remained low to fair, with *Kappa* values below 0.40 (Table S12).

Table 3
F and P *values of three-way permutational multivariate analysis of variance for the effects of genotype (G), inoculation (I), treatment (T), and their interaction* (i.e., *'G' × 'I', 'G' × 'T', 'I' × 'T', 'G' × 'I' × 'T') on the full-range (400–2,400 nm) reflectance profiles of wheat plants collected at ground-canopy level at 2, 5 and 14 days post inoculation (dpi).* df *represents degrees of freedom.* *** P ≤ *0.001,* ** P ≤ *0.01,* * P ≤ *0.05; ns:* P > *0.05.*

TIME	*EFFECT*	*df*	F	*P*
2 dpi	G	1	0.65	ns
	I	1	0.67	ns
	T	2	1.74	ns
	G × I	1	0.66	ns
	G × T	2	1.59	ns
	I* × *T	***2***	***3.02***	*
	G × I × T	2	1.38	ns
5 dpi	**G**	**1**	**10.70**	***
	I	1	0.99	ns
	T	**2**	**3.52**	**
	G × I	1	2.03	ns
	G × T	2	0.98	ns
	I × T	2	0.26	ns
	G* × *I* × *T	***2***	***3.73***	**
14 dpi	**G**	**1**	**3.85**	**
	I	1	0.37	ns
	T	**2**	**2.91**	*
	G × I	1	1.18	ns
	G* × *T	***2***	***4.62***	**
	I × T	2	1.25	ns
	G × I × T	2	0.98	ns

3.4. PLSR prediction models from leaf spectra

To optimize PLSR prediction of leaf physiological and biochemical traits, several spectral regions and different numbers of components, i.e., latent variables, were tested for each target variable, including A, E, g_s, C_i, WUE_i, WUE_{in}, Chl_{SPAD}, Ψ_w, and Ψ_π. Candidate spectral regions included the full 400–2400 nm range and narrower VIS, NIR, and SWIR windows selected according to known absorption features reported in the literature and their expected direct or indirect relationships with the measured traits. The final models were selected to maximize prediction accuracy, namely the highest R^2 and the lowest RMSE, %RMSE, and bias, as reported in Table S13. The final models for the prediction of A, g_s, and C_i used the range 400–2400 nm. For WUE_i and WUE_{in}, the best results were obtained by using the range 950–2400 nm. The 400–900 nm range was utilized in the final PLSR models for the prediction of Chl_{SPAD} and E. The final model for Ψ_π used the range 1300–2400 nm. Lastly, for Ψ_W, the best accuracy was obtained by using the 400–1200 nm range (Table 4). High prediction accuracy was achieved for Chl_{SPAD} and Ψ_π (R^2: 0.84 and 0.70, respectively), whereas A showed moderate-to-good validation accuracy (R^2: 0.63). Moderate prediction accuracy was obtained for g_s, C_i, WUE_i, and WUE_{in} (R^2: 0.45, 0.55, 0.47 and 0.52, respectively). Finally, insufficient accuracy ($R^2 < 0.30$) was obtained for E and Ψ_W and were therefore not considered reliably estimable from leaf reflectance in the present dataset. Statistics about PLSR models are reported in Figs. 4 and 5. External-validation fit statistics were reported only for primary measured traits whose internal-validation performance reached R^2 val ≥ 0.50 (Table 5). Other parameters were excluded because of lower internal-validation performance, whereas WUE_i and WUE_{in} were not included because they are ratio-derived traits.

3.5. Vegetation indices and traits predicted from leaf spectra

Table 6 reports the effects of 'G', 'I', 'T' and their interactions on vegetation indices and selected leaf traits predicted from spectral data. Only traits predicted by PLSR models with a validation $R^2 \geq 0.60$ were considered. At 2 dpi, significant three-way interactions ('G' × 'I' × 'T') were detected for Ψ_π, NDLI, and NDWI (Fig. S2). At 5 dpi, a significant three-way interaction persisted for Ψ_π and was newly observed for NDVI (Fig. S3). Finally, at 14 dpi, significant 'G' × 'I' × 'T' interactions were detected for several traits, including Chl_{SPAD}, NDWI, NDVI, and sARI (Fig. S4).

To visualize these complex physiological shifts, hierarchical clustering was performed (Fig. 6). Consistent with the highly significant main effect of 'G' observed in Table 6 across almost all indices, the heatmaps reveal that the primary clustering factor at all time points was 'G', clearly separating Rebelde and Bingo. Within these genotypic clusters, the effects of treatment and infection became increasingly distinct over time. By 14 dpi (Fig. 6C), the patterns of upregulation and downregulation for traits like sARI and NDVI diverged notably between the two cultivars, visually corroborating the significant three-way interactions (i.e., 'G' × 'I' × 'T') and indicating that the physiological response to Bioc and Chem treatments was strictly genotype dependent.

4. Discussion

4.1. Spectral discrimination of wheat-FHB-Biol/Chem interactions

This study demonstrated the potential of full-range hyperspectral data (i.e., 400–2,400 nm) to accurately discriminate among different wheat cultivars and to capture the specific effects of different treatments under FHB infection, although classification performance should be interpreted cautiously given the low-to-fair validation *Kappa* values obtained by PLS-DA. Reflectance profiles proved highly sensitive to both infection and treatment conditions, enabling the separation of FHB- and FHB+ plants even before visible symptoms appeared. Notably, at the leaf level, spectral signatures allowed for discrimination between FHB+

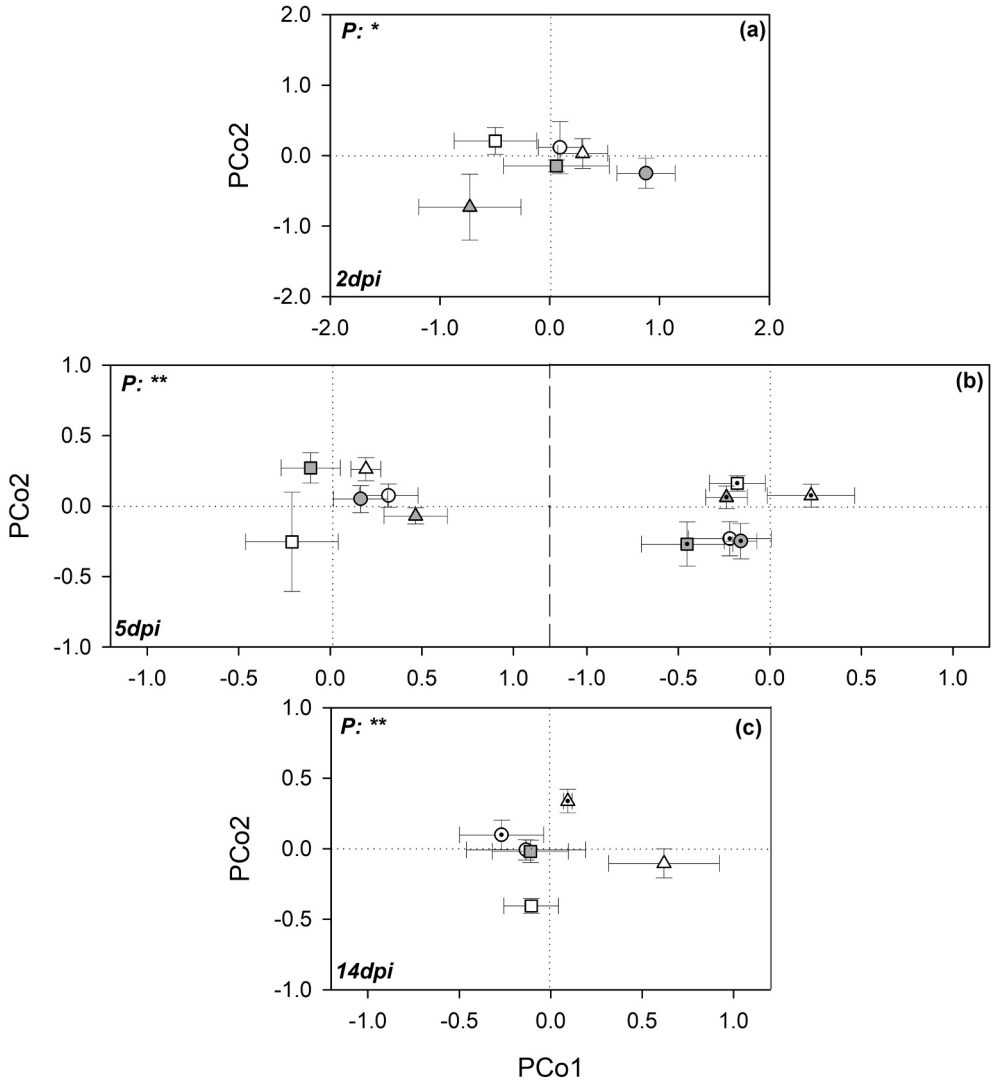

Fig. 3. *Scores (mean ± standard error) for the first and second principal components from principal coordinates analysis (PCoA) of reflectance data (400–2,400 nm) collected from wheat plants at ground-canopy level on Rebelde and Bingo winter wheat cultivars treated with water (Mock), systemic agrochemical (Chem) and* Trichoderma gamsii *T6085 (Bioc) and inoculated (FHB-) or not (FHB+) with* Fusarium graminearum *ITEM124 and* F. langsethiae *ITEM 11031 at two (**a**), five (**b**) and 14 (**c**) days post inoculation (dpi). (**a**) White and grey shapes represent scores for FHB- and FHB+ plants (regardless of the cultivar), respectively, treated with Mock (circles), Chem (square) and Bioc (triangles). (**b**) White and grey shapes represent scores for FHB- and FHB+ plants, respectively, treated with Mock (circles), Chem (square) and Bioc (triangles). Empty and dotted symbols represent the Rebelde and Bingo cultivar, (left and right sub-panel, separated by the dashed vertical line), respectively). (**c**) Shapes represent scores for plants treated with Mock (circles), Chem (square) and Bioc (triangles), regardless of the FHB inoculation. Empty and dotted symbols represent the Rebelde and Bingo cultivar.* P *value from permutational analysis of variance on full range (400–2,400 nm) reflectance profiles of wheat leaves are shown on the top right corner of panels (**: P ≤ 0.01; *: P ≤ 0.05).*

Table 4

Range of wavelengths, number of components (Com), model goodness-of-fit (R^2), root mean square error (RMSE), and percent RMSE of the data range (%RMSE) for calibration (Cal) and validation (Val) data generated using 500 random permutations of the data with 80 % used for Cal and 20 % used for the Val for the PLSR models predicting leaf physiological and biochemical traits wheat plants. Data are shown as mean ± standard deviation. Trait abbreviations: A, CO_2 assimilation rate ($\mu mol\ m^{-2}\ s^{-1}$); E, transpiration ($mmol\ m^{-2}\ s^{-1}$); g_s, leaf stomatal conductance to water vapor flux ($mol\ m^{-2}\ s^{-1}$);C_i, intercellular CO_2 concentration ($\mu mol\ mol^{-1}$); WUE_i, instantaneous water-use efficiency ($\mu mol\ mmol^{-1}$); WUE_{in}, intrinsic water-use efficiency ($\mu mol\ mol^{-1}$); Chl_{SPAD}, leaf greenness; Ψ_W, water potential (−MPa); Ψ_π, osmotic potential (−MPa).

Parameter	Range (nm)	Comp	Cal			Val			*Bias*
			R^2	RMSE	%RMSE	R^2	RMSE	%RMSE	
A	400–2,400	19	0.86 ± 0.01	2.11 ± 0.05	7	0.63 ± 0.16	3.50 ± 0.54	11	−0.17 ± 0.87
E	400–900	12	0.45 ± 0.07	2.16 ± 0.28	12	0.24 ± 0.13	2.7 ± 0.85	15	0.04 ± 1.58
g_s	400–2,400	12	0.63 ± 0.02	86.9 ± 2.28	12	0.45 ± 0.11	107 ± 10.40	15	−1.47 ± 19.46
C_i	400–2,400	16	0.77 ± 0.02	10.2 ± 0.35	11	0.55 ± 0.11	15 ± 1.60	15	0.22 ± 2.84
WUE_i	950–2,400	12	0.68 ± 0.03	0.22 ± 0.01	11	0.47 ± 0.11	0.29 ± 0.03	14	−0.00 ± 0.06
WUE_{in}	950–2,400	13	0.72 ± 0.02	6.06 ± 0.21	12	0.52 ± 0.10	8.12 ± 0.88	16	−0.17 ± 1.59
Chl_{SPAD}	400–900	11	0.89 ± 0.01	1.92 ± 0.05	4	0.84 ± 0.07	2.26 ± 0.22	5	−0.05 ± 0.44
Ψ_W	400–1,200	10	0.26 ± 0.03	0.17 ± 0.06	12	0.04 ± 0.15	0.21 ± 0.09	15	−0.00 ± 0.04
Ψ_π	1,300–2,400	14	0.82 ± 0.03	0.09 ± 0.00	11	0.70 ± 0.12	0.14 ± 0.02	17	−0.00 ± 0.03

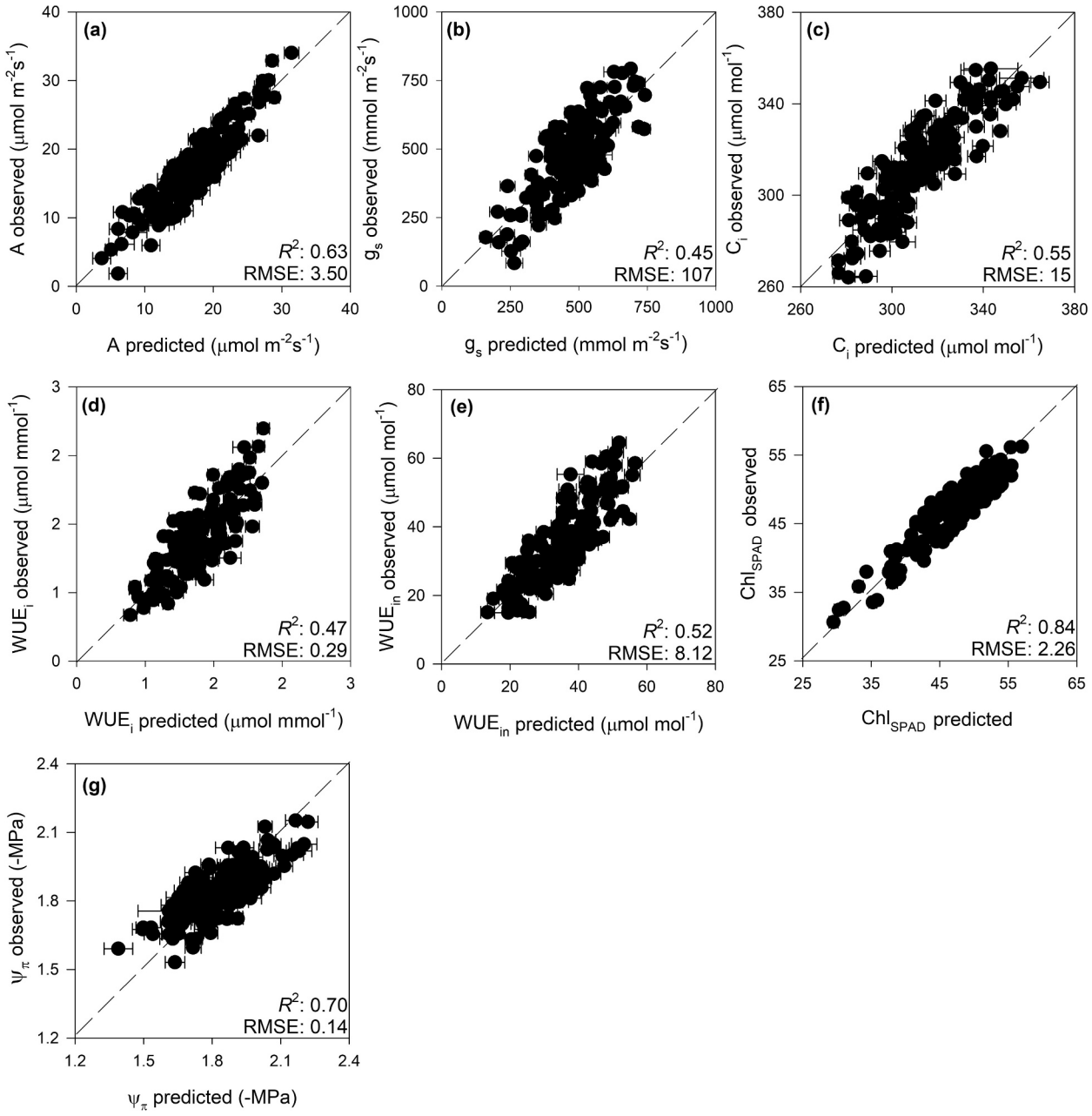

Fig. 4. Observed and partial least squares regression (PLSR)-predicted values of physiological and biochemical parameters in wheat leaves; error bars for predicted values represent the standard deviation generated from 500 simulated models; dashed line is 1:1 relationship; model goodness-of-fit (R^2), and root mean square error (RMSE) for validation data generated using 80 % of the data for calibration and 20 % for validation are reported. Bias outputs are not shown as they were always lower than 0.01. (**a**) A; (**b**) C_i; (**c**) g_s; (**d**) WUE_i; (**e**) WUE_{in}; (**f**) Chl_{SPAD}; (**g**) Ψ_π.

and FHB- plants at 2 dpi, independently of cultivar, while visible symptoms were only observed at 14 dpi in Mock/FHB+ Bingo plants (Risoli et al., 2025). These early spectral variations likely reflect infection-induced degradation in leaf pigments and water-related biochemical features, consistent with previous findings on biotic stress detection through hyperspectral reflectance (Merzlyak et al., 2003; Cotrozzi et al., 2018; Pippi et al., 2025). Thus, the multivariate spectral analyses were interpreted as indicators of treatment- and infection-dependent plant functional responses, rather than as purely statistical group separations.

At 5 dpi, the spectral analysis revealed significant 'G' effects and complex 'G' × 'I' × 'T' interactions, indicating that whole-spectrum profiles were sensitive to the combined influence of genotype, infection, and treatment. However, PLS-DA validation performance for these combined factors was low to fair, and the classification results should therefore be interpreted as an exploratory assessment of spectral class separability rather than as evidence of robust treatment discrimination. Some cultivar- or treatment-specific combinations showed higher class-specific accuracies in the confusion matrices, suggesting the presence of treatment-dependent spectral fingerprints. Nevertheless, these patterns remain insufficient to support practical discrimination of Chem and Bioc treatments without stronger classification performance and broader independent validation.. PLS-DA should therefore be interpreted as an exploratory assessment of spectral class separability rather than as a tool for operational discrimination of treatments.

Comparable results were obtained at the canopy-level, underscoring that hyperspectral sensing can capture infection- and treatment-related spectral patterns beyond the single-leaf scale. This finding supports the

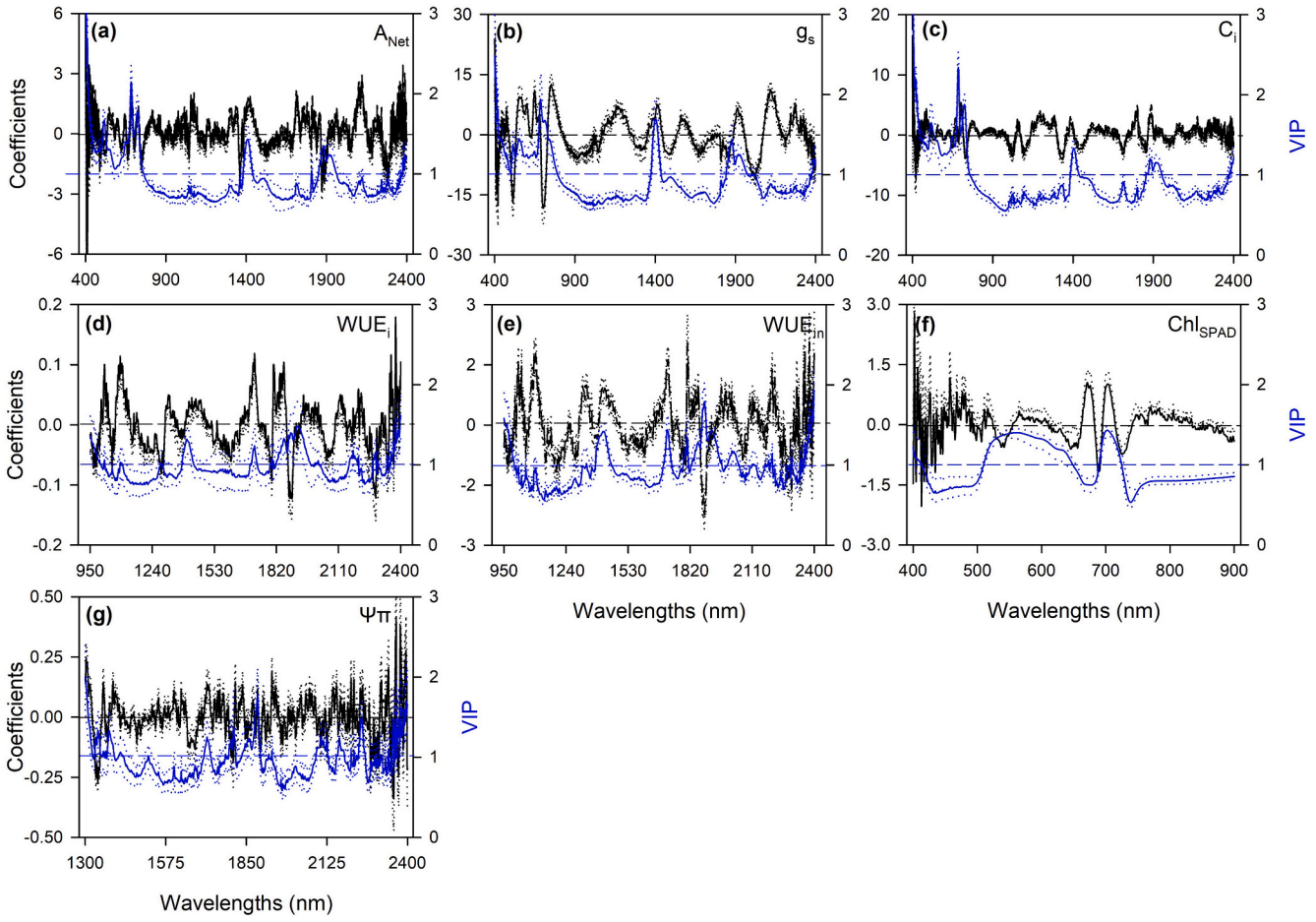

Fig. 5. Mean (solid), 5th and 95th percentile (dotted) of standardized coefficients (black, y axis on the left) and variable importance for projection (VIP, blue, y axis on the right) by wavelengths for the PLSR models predicting physiological and biochemical parameters in wheat. (**a**) A; (**b**) C_i; (**c**) g_s; (**d**) WUE_i; (**e**) WUE_{in}; (**f**) Chl_{SPAD}; (**g**) Ψ_π.

Table 5
Range, model goodness-fit (R^2), root-mean square error (RMSE) and bias for external validation data generated using 500 random permutations of the data for PLSR-models predicting leaf traits from wheat spectra. Data are shown as mean ± standard deviation. For traits abbreviation see Table 4.

Parameters	Spectral region (nm)	R^2	RMSE	%RMSE	*Bias*
A	400–2,400	0.60	3.54	15.94	0.68
C_i	400–2,400	0.64	14.54	15.41	−2.61
Chl_{SPAD}	400–900	0.94	2.12	5.93	0.53
Ψ_π	1300–2,400	0.69	0.15	17.73	−0.06

sensitivity of full-range spectroscopy to infection- and treatment-related spectral patterns beyond the single-leaf scale, but also confirms that canopy-level classification should currently be considered exploratory rather than operational (Cotrozzi and Couture, 2020; Couture et al., 2018).

Despite partial misclassifications among samples with lower infection severity, possibly due to environmental variability or inherent resistance differences among cultivars, the spectral analysis detected early FHB-related variation and treatment-dependent spectral responses. However, the low-to-fair PLS-DA performance limits confidence in practical treatment classification at this stage. Overall, these results indicate that hyperspectral phenotyping can capture treatment- and genotype-dependent spectral responses within the wheat–FHB–biocontrol system, but its current use for discriminating Chem and Bioc treatments should be considered exploratory and requires further validation across environments, seasons, cultivars, and disease-pressure conditions.

4.2. Predictive modeling of physiological and biochemical leaf traits

A key outcome of this work is the concomitant estimation of multiple gas-exchange, water-status, and pigment-related traits from hyperspectral data, despite the extremely challenging experimental setting (i.e., open-field conditions, complex tri-trophic interaction, and heterogeneous infection pressure). Using PLSR (Wold et al., 2001), we screened spectral windows and latent-variable numbers to maximize prediction accuracy (i.e., highest R^2, lowest RMSE, %RMSE, bias). The final leaf-level models leveraged trait-specific regions: 400–2,400 nm for A, g_s, and C_i; 950–2,400 nm for WUE_i and WUE_{in}; 400–900 nm for Chl_{SPAD} and E; 1,300–2,400 nm for Ψ_π; and 400–1,200 nm for Ψ_W. Notably, Chl_{SPAD} and Ψ_π achieved high validation accuracy ($R^2 = 0.84$ and 0.70, respectively), A performed well ($R^2 = 0.63$), g_s, C_i, WUE_i, WUE_{in} were medium ($R^2 = 0.45$–0.55), whereas E and Ψ_W were insufficient ($R^2 < 0.30$). External validations were consistent for A, C_i, WUE_{in}, Chl_{SPAD}, and Ψ_π, supporting model robustness under data partitioning. However, the utility of these models should be interpreted according to trait-specific validation performance. While Chl_{SPAD} and Ψ_π were predicted with sufficient accuracy for robust non-destructive phenotyping, the moderate validation performance of A, C_i, WUE_i, and WUE_{in} indicates that these estimates are more suitable for detecting relative treatment- or genotype-dependent trends than for precise absolute quantification. In contrast, the low validation R^2 values obtained for E and Ψ_w indicate that these traits cannot be reliably estimated from

Table 6
F *and* P *levels (*** P ≤ 0.001, ** P ≤ 0.01, * P ≤ 0.05; ns: P > 0.05) of three-way repeated measures of variance (ANOVA) for the effects of genotype (G), inoculation (I), treatment (T), and their interaction* (i.e., *'G' × 'I', 'G' × 'T', 'I' × 'T' and 'G' × 'I' × 'T') on leaf traits and spectral indices calculated from wheat spectra collected at leaf level at 2, 5 and 14 days post inoculation (dpi). df represents degrees of freedom. For traits abbreviation see Table 4. Indices abbreviations: NDLI, normalized difference lignin index; NDVI, normalized difference vegetation index; NDWI, normalized difference water index; sARI, anthocyanins reflectance index (scaled).*

Time (dpi)	Index	G (df: 1)	I (df: 1)	T (df:2)	G × I (df:2)	G × T (df:2)	I × T (df:2)	G × I × T (df:2)
2	**A**	12.40***	1.50 *ns*	0.15 *ns*	0.68 *ns*	0.35 *ns*	4.23*	0.23 *ns*
	C_i	40.54***	9.01**	3.21 *ns*	1.66 *ns*	1.02 *ns*	3.22*	0.53 *ns*
	Chl_{SPAD}	9.89**	0.20 *ns*	0.42 *ns*	0.23 *ns*	0.66 *ns*	1.28 *ns*	1.09 *ns*
	Ψ_π	0.53 *ns*	3.96*	9.83***	4.49*	7.01**	10.06***	**4.81****
	NDWI	95.46***	0.80 *ns*	22.22***	0.31 *ns*	1.47 *ns*	19.00***	**3.54***
	NDVI	51.17***	0.46 *ns*	0.26 *ns*	0.88 *ns*	1.45 *ns*	3.04 *ns*	2.77 *ns*
	NDLI	0.18 *ns*	9.33***	0.80 *ns*	1.08 *ns*	5.86**	1.71 *ns*	**3.37***
	sARI	6.01**	3.82 *ns*	0.55 *ns*	0.06 *ns*	1.43 *ns*	0.46 *ns*	2.84 *ns*
5	**A**	52.84***	1.17 *ns*	0.03 *ns*	0.44 *ns*	2.54 *ns*	1.56 *ns*	0.61 *ns*
	C_i	170.87***	0.15 *ns*	1.74 *ns*	1.02 *ns*	1.55 *ns*	3.65*	0.77 *ns*
	Chl_{SPAD}	16.75***	6.94**	0.07 *ns*	0.44 *ns*	0.14 *ns*	4.42*	1.82 *ns*
	Ψ_π	40.15***	0.01 *ns*	2.19 *ns*	0.06 *ns*	0.42 *ns*	0.44 *ns*	**3.95***
	NDWI	530.22***	0.83 *ns*	9.26**	0.17 *ns*	4.15*	3.74*	2.36 *ns*
	NDVI	115.32***	9.18**	0.12 *ns*	0.37 *ns*	2.37 *ns*	5.40*	**4.05***
	NDLI	1.27 *ns*	1.45 *ns*	0.11 *ns*	0.09 *ns*	0.21 *ns*	1.36 *ns*	0.08 *ns*
	sARI	38.21***	1.00 *ns*	0.09 *ns*	2.39 *ns*	3.85*	1.75 *ns*	1.57 *ns*
14	**A**	48.16***	5.48*	1.64 *ns*	6.36*	0.85 *ns*	3.47*	0.70 *ns*
	C_i	85.62***	0.04 *ns*	2.93 *ns*	4.67*	0.24 *ns*	1.62 *ns*	1.18 *ns*
	Chl_{SPAD}	76.02***	7.84***	3.10*	13.73***	0.86 *ns*	*0.09 ns*	**7.21*****
	Ψ_π	12.50***	0.02 *ns*	0.11 *ns*	1.80 *ns*	0.58 *ns*	0.67 *ns*	0.63 *ns*
	NDWI	882.42***	2.31 *ns*	9.92**	7.15***	31.74***	33.00***	**5.06****
	NDVI	346.27***	0.79 *ns*	30.20***	25.16***	2.56 *ns*	0.79 *ns*	**65.06*****
	NDLI	0.18 *ns*	0.70 *ns*	4.16*	0.81 *ns*	1.15 *ns*	9.08***	0.13 *ns*
	sARI	74.99***	0.36 *ns*	54.14***	8.81***	4.35*	2.27 *ns*	**4.80****

reflectance spectra under the present experimental conditions.

The wavelength dependence of the best models is mechanistically coherent with plant physiology. Chl_{SPAD} and E relied on VIS-NIR (400–900 nm), dominated by pigment absorption and red-edge dynamics-regions long linked to chlorophyll content and photosynthetic functioning (Gitelson et al., 2002; Gitelson and Merzlyak, 1994; Merzlyak et al., 1999). WUE_i and WUE_{in} performed best with NIR-SWIR (950–2,400 nm), where water and biochemical absorptions reflect the coupling between carbon assimilation and transpiration (Gamon et al., 1997; Gao, 1996; Serrano et al., 2002). Ψ_π peaked in the SWIR (1,300–2,400 nm), consistent with sensitivity to water and osmolyte signatures (e.g., carbohydrates, amino acids) that modulate osmotic potential (Cotrozzi et al., 2017; Cotrozzi and Couture, 2020). Conversely, the insufficient performance for Ψ_W and E indicates that these traits were not reliably estimable from leaf reflectance in the present dataset, likely because they are strongly influenced by short-term hydraulic regulation, stomatal dynamics, and microclimatic variability (Tiekstra et al., 2000). VIP profiles and standardized coefficients emphasized pigment-rich VIS bands and SWIR features (around 1,400–2,300 nm), aligning with prior evidence that these regions capture water content and nitrogen/ non-structural carbohydrates –related chemistry shaping Ψ_π and carbon–water trade-offs (Serbin et al., 2015; Cotrozzi et al., 2017; Cotrozzi and Couture, 2020).

Crucially, these accuracies were obtained while plants experienced complex tri-trophic interactions under open-field conditions, where infection dynamics, cultivar background, and Bioc/Chem treatments covaried. That the models retained skill for A, Ψ_π, and Chl_{SPAD} under such noise underscores the operational value of spectroscopy for rapid, non-destructive phenotyping in disease-challenged cereal systems (Mahlein et al., 2012, 2024; Alisaac and Mahlein, 2023). Although our quantitative modeling focused on leaf-level spectra, the same trait-wavelength logic extends to canopy-level sensing, where continuous reflectance/ fluorescence streams have been shown to track photosynthetic capacity and water dynamics (Gamon et al., 1995; Cogliati et al., 2015; Serbin et al., 2015). This scalability is particularly relevant for in-season decision support in FHB management, complementing early detection efforts (Bauriegel et al., 2011; Mustafa et al., 2022) and integrative monitoring under climate-amplified disease risks (Casu et al., 2024; Kos et al., 2023).

In Summary, the utility of these PLSR models was clearly trait-dependent: Chl_{SPAD} and Ψ_π were predicted with sufficient accuracy for robust non-destructive phenotyping, A, C_i, WUE_i, and WUE_{in} should be interpreted mainly as relative indicators of treatment- or genotype-dependent trends, whereas E and Ψ_w were not reliably estimable from leaf reflectance in the present dataset.

4.3. Variations of leaf spectra-estimated parameters and vegetation spectral indices

Finally, vegetation indices, spectra-derived traits, and clustering provided the physiological layer needed to interpret the spectral patterns identified by PERMANOVA and PLS-DA, highlighting early and dynamic plant responses to FHB infection and different treatments under field conditions. The variations observed in Chl_{SPAD} and Ψ_π and in several spectral indices (i.e., NDVI, NDWI, NDLI and sARI) clearly reflected both the infection progression and the cultivar- and treatment-specific responses. Already at 2 dpi, Ψ_π, NDLI and NDWI were significantly modulated by the full interaction among 'G', 'I', and 'T', indicating that even before visible symptoms, changes in osmotic adjustment and water-related indices could discriminate among infection and treatment combinations. NDLI and NDWI appeared especially sensitive to 'I' and 'T', in agreement with previous studies linking lignin- and water-related spectral features to pathogen-induced stress and host defense activation (Bauriegel et al., 2011; Cotrozzi et al., 2017; Mustafa et al., 2022).

At 5 dpi, Ψ_π and NDVI remained strongly affected by the tri-trophic interaction, while NDWI and C_i also responded to the combined effects of 'I' and 'T'. The strong 'G' effect on A and C_i across all time points confirmed cultivar-specific physiological behavior under stress, with Rebelde maintaining higher photosynthetic efficiency and osmotic stability than Bingo, which exhibited an earlier decline in Ψ_π and NDVI under infection. The influence of the Bioc treatment was also evident, as Bioc-treated plants, particularly Rebelde, displayed higher NDWI values compared to the Chem and Mock treatments, suggesting improved water

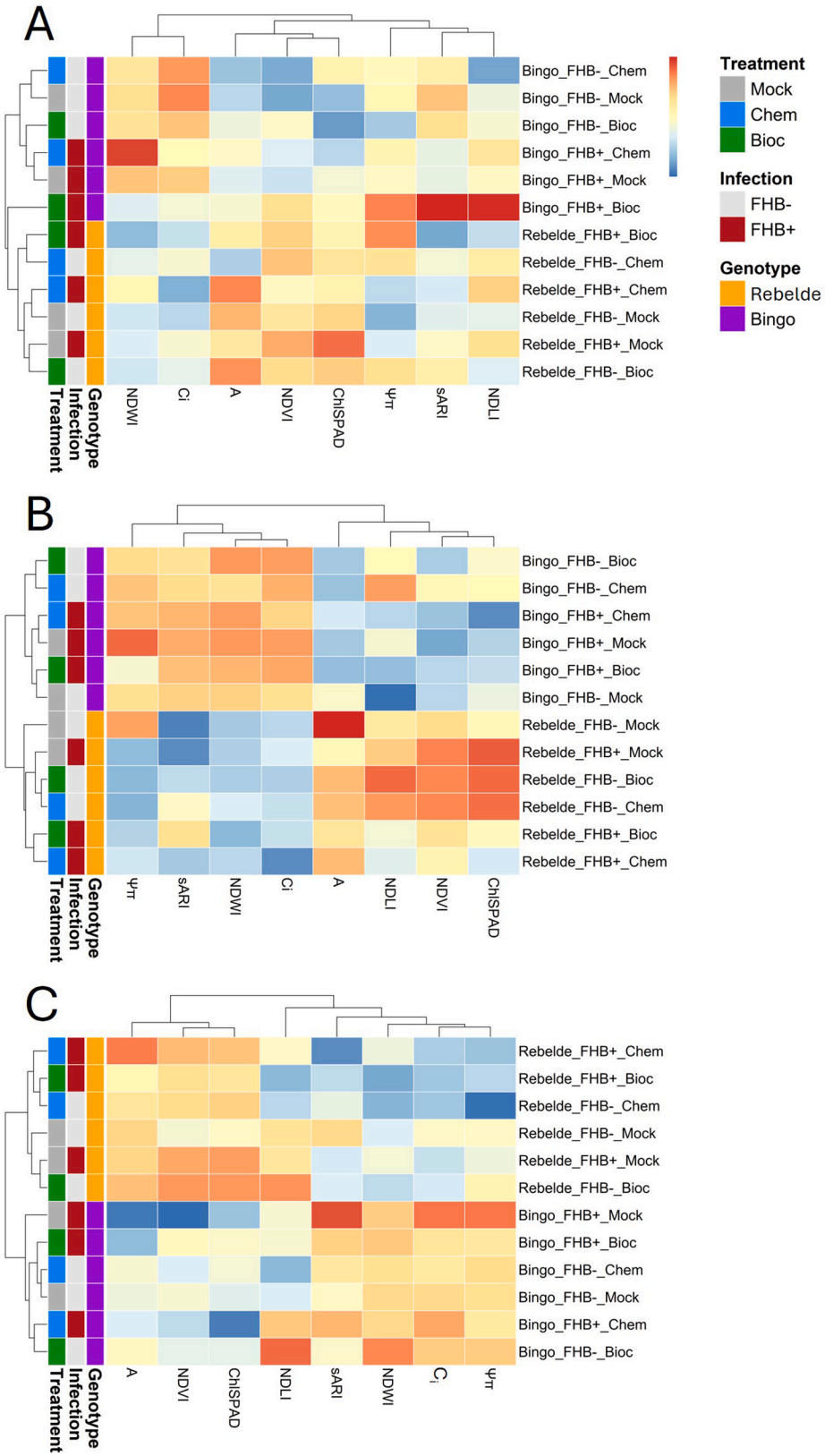

Fig. 6. Heatmaps illustrate the mean response profiles of Rebelde and Bingo winter wheat cultivars at 2 (A), 5 (B), and 14 (C) days post-inoculation (dpi). The values for each parameter (columns) were standardized as Z-scores to allow comparison between different units of measurement. The color gradient indicates the relative magnitude of the values: red represents values above the column mean, while blue represents values below the mean. Hierarchical clustering was applied to both rows (experimental treatments) and columns (parameters) to highlight similar response patterns. The colored annotation bars on the left identify the experimental factors: Genotype (Rebelde, orange; Bingo, purple), Infection (FHB-, light grey; FHB+, red) and Treatment (Mock, dark grey; Chem, blue; Bioc, green). For traits and indices abbreviation see Table 4 and Table 6, respectively.

status and enhanced photoprotective capacity-responses consistent with *Trichoderma*-mediated modulation of stress physiology (Bonaterra et al., 2022; Risoli et al., 2023, 2025).

By 14 dpi, the cumulative effects of infection and treatment were reflected in multiple indices and traits, including Chl_{SPAD}, NDVI, NDWI, and sARI, all significantly influenced by the three-way interaction. NDVI and NDWI were dominated by strong 'G' and 'T' effects, indicating that differences in leaf structure, pigment content, and water relations were key determinants of the wheat spectral response to FHB. Infected plants, particularly in the Bingo-Mock combination, showed lower NDVI values, consistent with chlorophyll degradation and early senescence. Similarly, the strong variation of sARI at 14 dpi reflected the activation of secondary metabolism, supporting an antioxidant response to infection and treatment effects (Ainsworth and Gillespie, 2007; Cotrozzi and Couture, 2020; Risoli et al., 2025).

Overall, these results confirm that spectral indices and modeled physiological parameters jointly trace the multifactorial nature of plant responses to FHB under open-field conditions. The early spectral deviations in Ψ_π, NDLI and NDWI demonstrate that hyperspectral sensing can detect subtle functional shifts in wheat long before visible damage occurs. The cultivar-dependent responses to Bioc and Chem treatments further underline the importance of integrating genotype-specific and environmentally driven factors into predictive disease management strategies (McMullen et al., 2012; Alisaac and Mahlein, 2023).

5. Conclusion

This study demonstrates that full-range hyperspectral sensing can effectively detect and characterize the early physiological, biochemical, and structural responses of wheat to FHB infection under field conditions. Through a combined approach of whole-spectrum analysis, exploratory classification, classification and PLSR modeling, we successfully discriminated between infected and healthy plants as early as 2 dpi and accurately predicted selected functional traits (i.e., photosynthetic and water-status parameters) from reflectance spectra with trait-dependent accuracy. The strong performance of Chl_{SPAD}, Ψ_π, and A models, together with the consistent sensitivity of NDVI and NDWI to infection and treatment, highlights the power of hyperspectral analysis for monitoring plant health beyond visible symptom appearance. However, E and Ψ_w could not be reliably estimated from reflectance in this dataset, indicating that the predictive utility of the approach was strongly trait-dependent. Similarly, while the proposed workflow is scalable as an experimental and analytical framework, its operational deployment will require broader validation across sites, seasons, cultivars, disease-pressure conditions, and sensing platforms.

In addition, our results indicate that FHB infection and management treatments induced genotype-dependent spectral and physiological responses, which were detectable at both leaf and canopy level in the present experimental system.. The distinct responses of Bingo and Rebelde further indicate that host susceptibility can influence spectral and physiological responses to FHB infection and treatment, although broader genotype-level conclusions will require validation across a wider set of cultivars.. Bioc treatment enhanced the resilience of both cultivars, maintaining higher water content and pigment stability, consistent with its known role in inducing stress tolerance.

The ability of hyperspectral reflectance to provide non-destructive, rapid, and integrative measurements of multiple functional traits represents a key advancement for precision phenotyping and disease management. By capturing early infection dynamics and treatment effects, this approach can support more sustainable and data-driven decisions in wheat production systems increasingly threatened by FHB and climate-driven stressors. The main limitations of the present study include the single-site and single-season design, the use of two cultivars, trait-dependent model performance, the need for quality-control outlier screening, and the potential influence of residual environmental variability on field spectral measurements. Future developments integrating hyperspectral data with thermal and fluorescence information will likely enhance predictive accuracy and enable real-time monitoring of crop-pathogen-environment interactions. Ultimately, our findings emphasize that vegetation spectroscopy can serve as a cornerstone for early warning systems, supporting both fundamental understanding and practical management of cereal diseases under real conditions.

CRediT authorship contribution statement

Lorenzo Pippi: Writing – original draft, Investigation, Formal analysis. **Samuele Risoli:** Writing – original draft, Formal analysis, Data curation, Conceptualization. **Sergio Cogliati:** Writing – review & editing, Supervision, Conceptualization. **Matteo Sali:** Writing – review & editing, Investigation, Formal analysis. **Roberto Garzonio:** Writing – review & editing, Investigation, Formal analysis. **Elisa Pellegrini:** Writing – review & editing, Supervision. **Cristina Nali:** Writing – review & editing, Supervision, Conceptualization. **Lorenzo Cotrozzi:** Writing – review & editing, Supervision, Conceptualization.

Funding

This paper and related research have been conducted during and with the support of the the project "Development of a MUlti-SEnsor remote sensing approach from drone to earLY detect plant diseases: A tool for sustainable agriculture and food security (MUSELY)" funded by the MUR PRIN 2022 PNRR (project#: P20228YXRE).

Declaration of competing interest

The authors declare that they have no known competing financial interests or personal relationships that could have appeared to influence the work reported in this paper.

Acknowledgements

This publication was produced while attending the PhD program in PhD in Sustainable Development And Climate Change at the University School for Advanced Studies IUSS Pavia, Cycle XXXVIII, with the support of a scholarship financed by the Ministerial Decree no. 351 of 9th April 2022, based on the NRRP–funded by the European Union – NextGenerationEU – Mission 4 "Education and Research", Component 1 "Enhancement of the offer of educational services: from nurseries to universities"–Investment 4.1 "Extension of the number of research doctorates and innovative doctorates for public administration and cultural".

Data availability

Data will be made available on request.

References

Agrawal, A.A., 2000. Mechanisms, ecological consequences and agricultural implications of tri-trophic interactions. Curr. Opin. Plant Biol. 3 (4), 329–335. https://doi.org/10.1016/S1369-5266(00)00089-3.

Ainsworth, E.A., Gillespie, K.M., 2007. Estimation of total phenolic content and other oxidation substrates in plant tissues using Folin–Ciocalteu reagent. Nat. Protoc. 2 (4), 875–877. https://doi.org/10.1038/nprot.2007.102.

Alisaac, E., Mahlein, A.K., 2023. Fusarium head blight on wheat: biology, modern detection and diagnosis and integrated disease management. Toxins 15 (3), 192. https://doi.org/10.3390/toxins15030192.

Altman, N., Krzywinski, M., 2017. Points of significance: clustering. Nat. Methods 14 (6), 545–547. https://doi.org/10.1038/nmeth.4299.

Anderson, M.J., 2001. A new method for non-parametric multivariate analysis of variance. Austral Ecol. 26 (1), 32–46. https://doi.org/10.1111/j.1442-9993.2001.tb00081.x.

Bauriegel, E., Giebel, A., Geyer, M., Schmidt, U., Herppich, W.B., 2011. Early detection of *Fusarium* infection in wheat using hyper-spectral imaging. Comput. Electron. Agric. 75 (2), 304–312. https://doi.org/10.1016/j.compag.2010.12.006.

Bonaterra, A., Badosa, E., Daranas, N., Francés, J., Roselló, G., Montesinos, E., 2022. Bacteria as biological control agents of plant diseases. Microorganisms 10 (9), 1759. https://doi.org/10.3390/microorganisms10091759.

Briglia, N., Williams, K., Wu, D., Li, Y., Tao, S., Corke, F., Montanaro, G., Petrozza, A., Amato, D., Cellini, F., Doonan, J.H., 2020. Image-based assessment of drought response in grapevines. Front. Plant Sci. 11, 595. https://doi.org/10.3389/fpls.2020.00595.

Butt, T.M., Copping, L.G., 2000. Fungal biological control agents. Pestic. Outlook 11 (5), 186–191. https://doi.org/10.1007/978-94-007-6380-7_3.

Carli, M., Pedrelli, A., Pippi, L., Risoli, S., Panattoni, A., Lorenzini, G., Pellegrini, E., Nali, C., Cotrozzi, L., 2025. Using leaf hyperspectral data to early detect flavescence dorée before the onset of symptoms in a heavily affected vineyard of Tuscany (Central Italy). Plant Dis. https://doi.org/10.1094/PDIS-04-25-0831-RE.

Casu, A., Camardo Leggieri, M., Toscano, P., Battilani, P., 2024. Changing climate, shifting mycotoxins: a comprehensive review of climate change impact on mycotoxin contamination. Compr. Rev. Food Sci. Food Saf. 23 (2), e13323. https://doi.org/10.1111/1541-4337.13323.

Chen, S., Hong, X., Harris, C.J., Sharkey, P.M., 2004. Sparse modeling using orthogonal forward regression with PRESS statistic and regularization. IEEE Transactions on Systems, Man, and Cybernetics, Part B (cybernetics) 34 (2), 898–911. https://doi.org/10.1109/tsmcb.2003.817107.

Chevallier, S., Bertrand, D., Kohler, A., Courcoux, P., 2006. Application of PLS-DA in multivariate image analysis. J. Chemom. 20 (5), 221–229. https://doi.org/10.1002/cem.994.

Chong, I.G., Jun, C.H., 2005. Performance of some variable selection methods when multicollinearity is present. Chemom. Intel. Lab. Syst. 78 (1–2), 103–112. https://doi.org/10.1016/j.chemolab.2004.12.011.

Cogliati, S., Rossini, M., Julitta, T., Meroni, M., Schickling, A., Burkart, A., Pinto, F., Rascher, U., Colombo, R., 2015. Continuous and long-term measurements of reflectance and sun-induced chlorophyll fluorescence by using novel automated field spectroscopy systems. Remote Sens. Environ. 164, 270–281. https://doi.org/10.1016/j.rse.2015.03.027.

Cotrozzi, L., Couture, J.J., 2020. Hyperspectral assessment of plant responses to multi-stress environments: prospects for managing protected agrosystems. Plants People Planet 2 (3), 244–258. https://doi.org/10.1002/ppp3.10080.

Cotrozzi, L., 2022. Spectroscopic detection of forest diseases: a review (1970–2020). J. For. Res. 33 (1), 21–38. https://doi.org/10.1007/s11676-021-01378-w.

Cotrozzi, L., Couture, J.J., Cavender-Bares, J., Kingdon, C.C., Fallon, B., Pilz, G., Pellegrini, E., Nali, C., Townsend, P.A., 2017. Using foliar spectral properties to assess the effects of drought on plant water potential. Tree Physiol. 37 (11), 1582–1591. https://doi.org/10.1093/treephys/tpx106.

Cotrozzi, L., Peron, R., Tuinstra, M.R., Mickelbart, M.V., Couture, J.J., 2020. Spectral phenotyping of physiological and anatomical leaf traits related with maize water status. Plant Physiol. 184 (3), 1363–1377. https://doi.org/10.1093/treephys/tpx106.

Cotrozzi, L., Townsend, P.A., Pellegrini, E., Nali, C., Couture, J.J., 2018. Reflectance spectroscopy: a novel approach to better understand and monitor the impact of air pollution on Mediterranean plants. Environ. Sci. Pollut. Res. 25, 8249–8267. https://doi.org/10.1007/s11356-017-9568-2.

Couture, J.J., Singh, A., Charkowski, A.O., Groves, R.L., Gray, S.M., Bethke, P.C., Townsend, P.A., 2018. Integrating spectroscopy with potato disease management. Plant Dis. 102 (11), 2233–2240. https://doi.org/10.1094/pdis-01-18-0054-re.

Dean, R., Van Kan, J.A., Pretorius, Z.A., Hammond-Kosack, K.E., Di Pietro, A., Spanu, P. D., Rudd, J.J., Dickman, M., Kahmann, R., Ellis, J., Foster, G.D., 2012. The top 10 fungal pathogens in molecular plant pathology. Mol. Plant Pathol 13 (4), 414–430. https://doi.org/10.1111/j.1364-3703.2012.2011.00783.x.

Dixon, P., 2003. VEGAN, a package of R functions for community ecology. J. Veg. Sci. 14 (6), 927–930. https://doi.org/10.1658/1100-9233(2003)014[0927:vaporf]2.0.co;2.

Dweba, C.C., Figlan, S., Shimelis, H.A., Motaung, T.E., Sydenham, S., Mwadzingeni, L., Tsilo, T.J., 2017. Fusarium head blight of wheat: Pathogenesis and control strategies. Crop Prot. 91, 114–122. https://doi.org/10.1016/j.cropro.2016.10.002.

EFSA Panel on Contaminants in the Food Chain (CONTAM), Knutsen, H.K., Alexander, J., Barregård, L., Bignami, M., Brüschweiler, B., Ceccatelli, S., Cottrill, B., Dinovi, M., Grasl-Kraupp, B., Hogstrand, C., 2017. Risks to human and animal health related to the presence of deoxynivalenol and its acetylated and modified forms in food and feed. *EFSA journal*, *15*(9), e04718. Doi: 10.2903/j.efsa.2014.3916.

Erenstein, O., Jaleta, M., Mottaleb, K.A., Sonder, K., Donovan, J., Braun, H.J., 2022. Global trends in wheat production, consumption and trade. In *Wheat improvement: food security in a changing climate* (pp. 47-66). Cham: Springer International Publishing. Doi: 10.1007/978-3-030-90673-3_4.

Gamon, J., Serrano, L., Surfus, J.S., 1997. The photochemical reflectance index: an optical indicator of photosynthetic radiation use efficiency across species, functional types, and nutrient levels. Oecologia 112, 492–501. https://doi.org/10.1007/s004420050337.

Gamon, J.A., Field, C.B., Goulden, M.L., Griffin, K.L., Hartley, A.E., Joel, G., Penuelas, J., Valentini, R., 1995. Relationships between NDVI, canopy structure, and photosynthesis in three californian vegetation types. Ecol. Appl. 5 (1), 28–41. https://doi.org/10.2307/1942049.

Gao, B.C., 1996. NDWI—A normalized difference water index for remote sensing of vegetation liquid water from space. Remote Sens. Environ. 58 (3), 257–266. https://doi.org/10.1016/s0034-4257(96)00067-3.

Gitelson, A.A., Merzlyak, M.N., Chivkunova, O.B., 2001. Optical properties and nondestructive estimation of anthocyanin content in plant leaves. Photochem. Photobiol. 74 (1), 38–45. https://doi.org/10.1562/0031-8655(2001)0740038opaneo2.0.co2.

Gitelson, A., Merzlyak, M.N., 1994. Quantitative estimation of chlorophyll-*a* using reflectance spectra: Experiments with autumn chestnut and maple leaves. J. Photochem. Photobiol. B Biol. 22 (3), 247–252. https://doi.org/10.1016/1011-1344(93)06963-4.

Gitelson, A.A., Zur, Y., Chivkunova, O.B., Merzlyak, M.N., 2002. Assessing carotenoid content in plant leaves with reflectance spectroscopy. Photochem. Photobiol. 75 (3), 272–281. https://doi.org/10.1562/0031-8655(2002)0750272accipl2.0.co2.

Gongora-Canul, C., Salgado, J.D., Singh, D., Cruz, A.P., Cotrozzi, L., Couture, J., Rivadeneira, M.G., Cruppe, G., Valent, B., Todd, T., Poland, J., 2020. Temporal dynamics of wheat blast epidemics and disease measurements using multispectral imagery. Phytopathology 110 (2), 393–405. https://doi.org/10.1094/phyto-08-19-0297-r.

Khan, M.K., Pandey, A., Athar, T., Choudhary, S., Deval, R., Gezgin, S., Hamurcu, M., Topal, A., Atmaca, E., Santos, P.A., Omay, M.R., 2020. Fusarium head blight in wheat: contemporary status and molecular approaches. 3 Biotech 10, 1–17. https://doi.org/10.3390/plants13162179.

Kos, J., Anić, M., Radić, B., Zadravec, M., Janić Hajnal, E., Pleadin, J., 2023. Climate change-a global threat resulting in increasing mycotoxin occurrence. Foods 12 (14), 2704. https://doi.org/10.3390/foods12142704.

Krska, R., Baumgartner, S., Josephs, R., 2001. The state-of-the-art in the analysis of type-a and-B trichothecene mycotoxins in cereals. Fresenius' Journal of Analytical Chemistry 371 (3), 285–299. https://doi.org/10.1007/s002160100992.

Kuhn, M., 2008. Building predictive models in R using the caret package. J. Stat. Softw. 28, 1–26. https://doi.org/10.18637/jss.v028.i05.

Lahlali, R., Ezrari, S., Radouane, N., Kenfaoui, J., Esmaeel, Q., El Hamss, H., Belabess, Z., Barka, E.A., 2022. Biological control of plant pathogens: a global perspective. Microorganisms 10 (3), 596. https://doi.org/10.3390/microorganisms10030596.

Legein, M., Smets, W., Vandenheuvel, D., Eilers, T., Muyshondt, B., Prinsen, E., Samson, R., Lebeer, S., 2020. Modes of action of microbial biocontrol in the phyllosphere. Front. Microbiol. 11, 1619. https://doi.org/10.3389/fmicb.2020.01619.

Mahlein, A.K., Arnal Barbedo, J.G., Chiang, K.S., Del Ponte, E.M., Bock, C.H., 2024. From detection to protection: the role of optical sensors, robots, and artificial Intelligence in modern plant disease management. Phytopathology 114 (8), 1733–1741. https://doi.org/10.1094/phyto-01-24-0009-per.

Mahlein, A.K., Oerke, E.C., Steiner, U., Dehne, H.W., 2012. Recent advances in sensing plant diseases for precision crop protection. Eur. J. Plant Pathol. 133, 197–209. https://doi.org/10.1007/s10658-011-9878-z.

McMullen, M., Bergstrom, G., De Wolf, E., Dill-Macky, R., Hershman, D., Shaner, G., Van Sanford, D., 2012. A unified effort to fight an enemy of wheat and barley: Fusarium head blight. Plant Dis. 96 (12), 1712–1728. https://doi.org/10.1094/pdis-03-12-0291-fe.

Merzlyak, M.N., Gitelson, A.A., Chivkunova, O.B., Rakitin, V.Y., 1999. Non-destructive optical detection of pigment changes during leaf senescence and fruit ripening. Physiol. Plant. 106 (1), 135–141. https://doi.org/10.1034/j.1399-3054.1999.106119.x.

Mustafa, G., Zheng, H., Khan, I.H., Tian, L., Jia, H., Li, G., Cheng, T., Tian, Y., Cao, W., Zhu, Y., Yao, X., 2022. Hyperspectral reflectance proxies to diagnose in-field fusarium head blight in wheat with machine learning. Remote Sens. (Basel) 14 (12), 2784. https://doi.org/10.3390/rs14122784.

Ons, L., Bylemans, D., Thevissen, K., Cammue, B.P., 2020. Combining biocontrol agents with chemical fungicides for integrated plant fungal disease control. Microorganisms 8 (12), 1930. https://doi.org/10.3390/microorganisms8121930.

Pippi, L., Alibani, M., Acito, N., Antichi, D., Caruso, G., Fontanelli, M., Moretti, M., Nali, C., Pampana, S., Pellegrini, E., Peruzzi, A., Risoli, S., Sileoni, G., Silvestri, N., Tramacere, L.G., Cotrozzi, L., 2025. Hyperspectral Detection of Single and combined Effects of simulated tree Shading and *Alternaria alternata* Infection on *Sorghum bicolor*, from Leaf to UAV-Canopy Scale. Agronomy 15 (11), 2458. https://doi.org/10.3390/agronomy15112458.

Pisuttu, C., Lo Piccolo, E., Paoli, L., Cotrozzi, L., Nali, C., Pellegrini, E., Lorenzini, G., 2023. Physiochemical responses of *Ailanthus altissima* under the challenge of *Verticillium dahliae*: Elucidating the decline of one of the world's worst invasive alien plant species. Biol. Invasions 25 (1), 61–78. https://doi.org/10.1007/s10530-022-02891-7.

Quaratiello, G., Risoli, S., Antichi, D., Pellegrini, E., Nali, C., Lorenzini, G., Pampana, S., Pisuttu, C., Tonelli, M., Cotrozzi, L., 2024. Exogenous melatonin application helps late-sown durum wheat to cope with waterlogging under Mediterranean environmental conditions. Physiol. Plant. 176 (4), e14477. https://doi.org/10.1111/ppl.14477.

Risoli, S., Cotrozzi, L., Sarrocco, S., Nuzzaci, M., Pellegrini, E., Vitti, A., 2022. Trichoderma-induced resistance to *Botrytis cinerea* in *Solanum* species: a Meta-Analysis. Plants 11 (2), 180. https://doi.org/10.3390/plants11020180.

Risoli, S., Petrucci, A., Vicente, I., Sarrocco, S., 2023. Trichoderma gamsii T6085, a biocontrol agent of Fusarium head blight, modulates biocontrol-relevant defence genes expression in wheat. Plant Pathol. 72 (8), 1442–1452. https://doi.org/10.1111/ppa.13773.

Risoli, S., Cotrozzi, L., Pisuttu, C., Nali, C., 2024. Biocontrol Agents of Fusarium Head Blight in Wheat: a Meta-Analytic Approach to Elucidate their Strengths and Weaknesses. Phytopathology 114 (3), 521–537. https://doi.org/10.1094/phyto-08-23-0292-r.

Risoli, S., García-Pérez, P., Quaratiello, G., Cotrozzi, L., Sarrocco, S., Pellegrini, E., Nali, C., Lorenzini, G., Lucini, L., 2025. Metabolomic insights on the response of winter wheat cultivars to Fusarium head blight infection and inoculation with a biocontrol strain in open field. Plant Stress 100807. https://doi.org/10.1016/j.stress.2025.100807.

Rypar, T., Risoli, S., Doppler, M., Bueschl, C., Seidl, B., Parich, A., Adam, G., Schuhmacher, R., 2025. Stable-isotope-assisted metabolomics enables the study of (a) biotic stress-related metabolism of tyrosine compared to phenylalanine in wheat. Plant Physiol. Biochem. 110214. https://doi.org/10.2139/ssrn.5203850.

Serbin, S.P., Singh, A., Desai, A.R., Dubois, S.G., Jablonski, A.D., Kingdon, C.C., Kruger, E.L., Townsend, P.A., 2015. Remotely estimating photosynthetic capacity, and its response to temperature, in vegetation canopies using imaging spectroscopy. Remote Sens. Environ. 167, 78–87. https://doi.org/10.1016/j.rse.2015.05.024.

Serrano, L., Penuelas, J., Ustin, S.L., 2002. Remote sensing of nitrogen and lignin in Mediterranean vegetation from AVIRIS data: Decomposing biochemical from structural signals. Remote Sens. Environ. 81 (2–3), 355–364. https://doi.org/10.1016/s0034-4257(02)00011-1.

Steiner, B., Buerstmayr, M., Michel, S., Schweiger, W., Lemmens, M., Buerstmayr, H., 2017. Breeding strategies and advances in line selection for Fusarium head blight resistance in wheat. Trop. Plant Pathol. 42, 165–174. https://doi.org/10.1007/s40858-017-0127-7.

Tiekstra, A.E., Else, M.A., Jackson, M.B., 2000. External pressures based on leaf water potentials do not induce xylem sap to flow at rates of whole plant transpiration from roots of flooded or well-drained tomato and maize plants. Impact of shoot hydraulic resistances. Ann. Bot. 86 (3), 665–674. https://doi.org/10.1006/anbo.2000.1193.

Wold, S., Sjöström, M., Eriksson, L., 2001. PLS-regression: a basic tool of chemometrics. Chemom. Intel. Lab. Syst. 58 (2), 109–130. https://doi.org/10.1016/s0169-7439(01)00155-1.